

Aminomethyl-Derived Beta Secretase (BACE1) Inhibitors: Engaging Gly230 without an Anilide Functionality

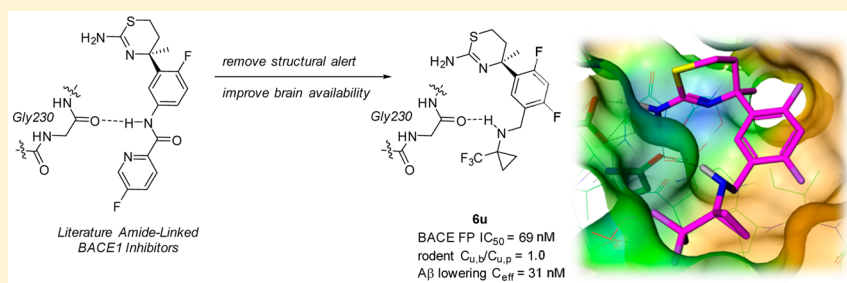
Christopher R. Butler,^{*,†,‡,§} Kevin Ogilvie,[§] Luis Martinez-Alsina,[§] Gabriela Barreiro,[†] Elizabeth M. Beck,[†] Charles E. Nolan,[‡] Kevin Atchison,[‡] Eric Benvenuti,[‡] Leanne Buzon,[§] Shawn Doran,[‡] Cathleen Gonzales,[‡] Christopher J. Helal,[§] Xinjun Hou,[†] Mei-Hui Hsu,[#] Eric F. Johnson,[#] Kimberly Lapham,[‡] Lorraine Lanyon,[‡] Kevin Parris,^{||} Brian T. O'Neill,[§] David Riddell,[‡] Ashley Robshaw,[‡] Felix Vajdos,^{||} and Michael A. Brodney[†]

[†]Neuroscience & Pain Medicinal Chemistry, [‡]Neuroscience & Pain Research Unit, Pfizer Worldwide Research and Development, 610 Main Street, Cambridge, Massachusetts 02139, United States

[§]Neuroscience & Pain Medicinal Chemistry, ^{||}Center of Chemistry Innovation and Excellence, [‡]Pharmacokinetics, Dynamics, and Metabolism, Pfizer Worldwide Research and Development, 445 Eastern Point Road, Groton, Connecticut 06340, United States

[#]Molecular and Experimental Medicine, The Scripps Research Institute, 10550 Torrey Pines Road, La Jolla, California 92024, United States

Supporting Information



ABSTRACT: A growing subset of β -secretase (BACE1) inhibitors for the treatment of Alzheimer's disease (AD) utilizes an anilide chemotype that engages a key residue (Gly230) in the BACE1 binding site. Although the anilide moiety affords excellent potency, it simultaneously introduces a third hydrogen bond donor that limits brain availability and provides a potential metabolic site leading to the formation of an aniline, a structural motif of prospective safety concern. We report herein an alternative aminomethyl linker that delivers similar potency and improved brain penetration relative to the amide moiety. Optimization of this series identified analogues with an excellent balance of ADME properties and potency; however, potential drug–drug interactions (DDI) were predicted based on CYP 2D6 affinities. Generation and analysis of key BACE1 and CYP 2D6 crystal structures identified strategies to obviate the DDI liability, leading to compound **16**, which exhibits robust in vivo efficacy as a BACE1 inhibitor.

INTRODUCTION

Alzheimer's disease (AD), a neurological disorder that imparts a slow progression of cognitive decline, dementia, and ultimately death, has yet to yield to a significant enhancement in treatment or prevention. Disease progression is marked by the deposition of amyloid β ($A\beta$)-derived plaques in the hippocampal and cortical regions of the brain. The amyloid hypothesis proposes that increased $A\beta$ production or its decreased clearance is responsible for the molecular cascade that eventually leads to neurodegeneration and AD.^{1,2} $A\beta$ production is initiated by the proteolytic cleavage of amyloid precursor protein (APP) by β -site APP cleaving enzyme (BACE1) within the endosome³ to afford a soluble N-terminal ectodomain of APP (sAPP β) and the C-terminal fragment C99.⁴ The membrane-bound C99 is then cleaved by γ -secretase to release $A\beta$, including $A\beta_{x-40}$ and $A\beta_{x-42}$ isoforms.⁵

Recently, an APP “loss of function” mutation, with protective effects against AD, has been reported to be cleaved more slowly by BACE1.⁶ Modulation of the $A\beta$ cascade via safe and effective inhibition of BACE1 has remained a target of great interest for a number of years.⁷

Considering the chronic dosing regimen required for a successful AD treatment, an exquisitely selective and safe profile for a BACE1 inhibitor is paramount. Of particular concern for this target is inhibition of hERG,⁸ as well as related aspartyl proteases including cathepsin D (CatD), which has confounded early generations of BACE1 inhibitors.⁹ The hERG-mediated cardiovascular liability is traditionally avoided by eliminating basic amine functionality and lowering lipophilicity.¹⁰ This is

Received: October 3, 2016

Published: December 6, 2016

challenging for BACE1, as the active site is most efficiently engaged through utilization of such an amine, thus requiring alternate mitigation strategies. Additionally, the binding sites of CatD and BACE1 have high sequence similarity, and therefore differentiation requires exploitation of subtle architectural variances in order to maintain affinity for BACE1 while avoiding CatD inhibition. Compounds that fail to achieve sufficient selectivity over CatD carry a liability for ocular toxicity due to the resulting accumulation of fluorescent material in the retinal pigment epithelium (RPE) layer.⁹

The physiological relevance of BACE2 has emerged in recent years, first as an enzyme involved in pigmentation processing, specifically acting on PMEL17 in the periphery.¹¹ Improper functioning of BACE2 is believed to result in hypopigmentation.¹² BACE2 is also expressed in the pancreas and plays a role in glucose homeostasis. To our knowledge, there are limited examples of BACE1 inhibitors possessing significant selectivity over BACE2. Compounds that lack this selectivity window and exhibit impaired access to the brain will therefore inherently suffer from significant inhibition of BACE2. In summary, agents developed for chronic BACE1 inhibition should be designed to minimize activity against related proteases such as CatD and BACE2.

The amidine-containing BACE1 inhibitors, reported by a number of groups, provide a suitable scaffold to systematically address the CatD and hERG liabilities.¹³ A number of these inhibitors, such as MK-8931 (**1**), have recently entered clinical studies; two of them are shown in Figure 1.¹⁴ A common

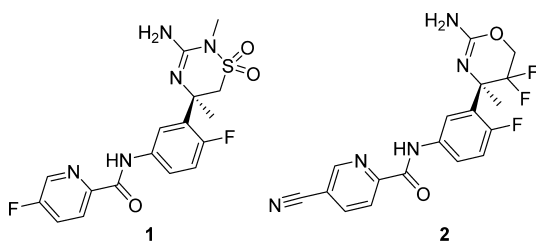


Figure 1. Selected literature BACE1 inhibitors.

construct within this class is an amide moiety connecting two aromatic rings that ultimately occupy the S1/S3 pockets when bound in the BACE1 active site. The incorporation of this moiety generally confers potent inhibition of BACE1 in addition to exquisite selectivity over CatD. Unfortunately, these merits are generally offset by increased P-gp-mediated efflux, resulting in decreased brain penetration. There is a correlation between the presence of a third hydrogen bond donor (HBD) and an increased likelihood of efflux transporter liabilities.¹⁵ Poor brain penetration inherently increases the body burden required to achieve the desired brain concentrations, and thus further exacerbates any issues arising from less than exquisite aspartyl protease selectivity. Moreover, recent reports have shown that there are relevant peripheral substrates for BACE1 in addition to the targeted central APP processing.¹⁶

Inhibitors bearing the P1/P3 amide motif not only exhibit higher efflux transporter liability but also contain a metabolic soft spot associated with amidase activity, which in this case would reveal anilines upon amide cleavage.¹⁷ In addition to this potential metabolic liability, anilines are themselves a structural alert, known to be a culprit for downstream toxicity associated either with oxidation of the electron-rich aryl ring and

subsequent trapping with ambient nucleophiles or oxidation of the nitrogen itself to the *N*-oxide.¹⁸

DESIGN CRITERIA

Despite a significant and sustained effort, the identification of a potent, safe, selective BACE1 inhibitor with a balanced ADME profile, including good brain penetration, remains challenging. Our design criteria were therefore to identify an orally efficacious BACE1 inhibitor that (a) demonstrates excellent selectivity (>100×) over hERG, CatD and the related aspartyl proteases, and (b) maintains good brain penetration ($C_{b,u}/C_{p,u}$ > 0.5 as measured in rodents) without the use of an anilide functionality.

We therefore sought to identify an amide replacement that provided the opportunity for similar efficiency gains while avoiding the potential for toxicity imparted by the buried aniline moiety. The recent BACE1 crystal structure of **2**, published by Roche, provides a structural rationale for the high inhibitory efficiency of P1/P3 amides (Figure 2).¹⁹ The amide

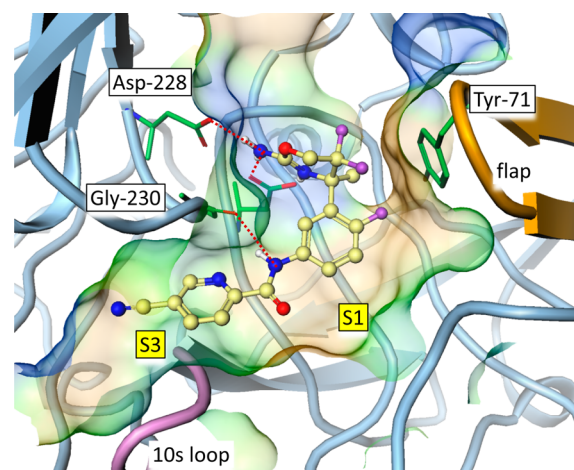


Figure 2. Interaction between Gly230 and **2** (PDB: 3ZMG, add 61 to residue numbers to match 3ZMG's number).

N-H is positioned at a near-ideal distance and angle to engage the backbone carbonyl of the Gly230 residue in a hydrogen bonding interaction. Additionally, the coplanar conformation of the rings occupying the S1/S3 pockets serves to efficiently fill the shallow lipophilic binding site.

Thus, a suitable amide replacement would need to fulfill these two structural requirements: effective engagement of Gly230 and reasonable concomitant occupation of the S1/S3 subpockets. Simple reversal of the amide removes the buried aniline while retaining the hydrogen bond donor, but rotation around the amide bond is then needed to recapitulate the optimum hydrogen bond angle, resulting in significant clashes with the edge of the S3 subpocket. In contrast, a homologated aminomethyl linker (Figure 3) addresses both of the aforementioned requirements. Among the salient features of this aminomethyl moiety, one key departure from the amide-derived analogues is its nonplanarity. The sp^3 nature of the benzylic carbon results in the two-atom unit preferring a nearly orthogonal orientation of the C–N bond relative to the fluorophenyl P1 ring, facilitating an optimal geometry for hydrogen bonding to Gly230. Optimization of the amine substituent in this alternative vector therefore becomes crucial to balance the interplay of requisite hydrogen-bond donating

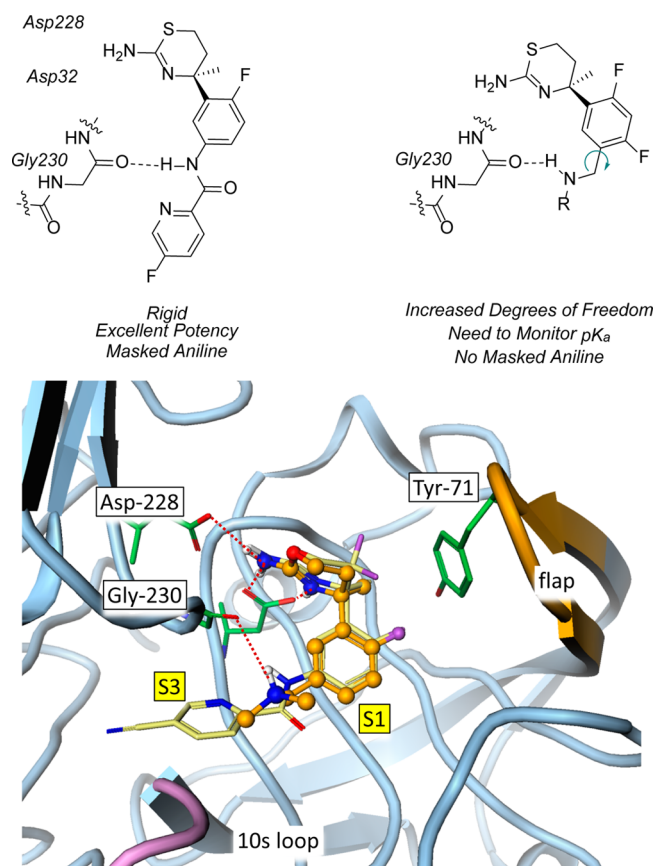


Figure 3. Strategy to mitigate challenges associated with amide linker pharmacophore of literature BACE inhibitors. Modeled alignment of aminomethyl design (orange) with compound 2 (yellow).

ability of the amine with the resultant ADME characteristics of these compounds.

RESULTS AND DISCUSSION

As it was not clear what structural attributes would be required to fill the S3 pocket in this new series, parallel (library) synthesis was employed to broadly evaluate structure–activity relationships for BACE1 inhibition. Compounds **6a–u** were prepared by the three-step protocol illustrated in Scheme 1. Formylation of the previously described bromide **3**²⁰ provided aldehyde **4**, which could be converted to the corresponding protected amidines **5** via a reductive amination with the requisite amines. Removal of the amidine protecting group using standard conditions provided the analogues of interest.

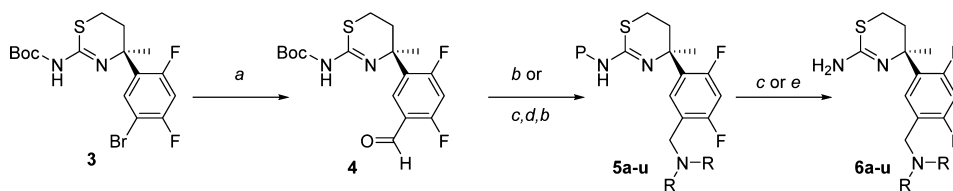
Analogues were evaluated in a panel of BACE1, BACE2, and CatD enzymatic assays (cell-free assay, CFA), as well as a whole-cell assay (WCA) reporting changes in soluble APP

(sAPP β) protein concentrations, indicative of APP processing by BACE1. The data from this assay panel, as well as key ADME parameters, for **6a–6k** are provided in Table 1. The direct replacement of the amide linker with an aminomethylene spacer, as exemplified by **6a**, yields weak activity at BACE1 (CFA IC₅₀ = 73.5 μ M), in stark contrast to the low nanomolar potency observed for many of the corresponding amides reported in the literature. In addition, the significant ADME challenges for this series are well illustrated by **6a**, which exhibits a high MDR efflux ratio (Er) and significant clearance in human liver microsomes (HLM). Analogues **6b–d**, which contain small alkyl substituents, show a modest improvement in BACE1 CFA potency, in concert with a dramatic increase in WCA potency (\sim 1000 \times shifted relative to the CFA) and excellent selectivity over CatD. The improvement is most marked when considering ligand and lipophilic efficiencies (LE, LipE) for these low molecular weight, polar, dibasic amine analogues. These compounds have significantly reduced clearance relative to **6a**, as measured by HLM, although they still exhibit significant P-gp transporter liability. Tertiary amines **6d–e** are significantly less active in the BACE1 CFA but still exhibit good potency in the WCA, albeit an overall decrease in LipE, relative to the secondary amines. Ether-containing substituents are also well tolerated (**6e,f**), showing similar potency in the WCA, low microsomal clearance but with modest to high efflux ratios. Introduction of a branched methyl group (**6c** vs **6b** and **6h** vs **6f**) offers an enhancement in potency (WCA) and a modest improvement in selectivity over BACE2. Tying this branching back into a 1,1,1-bicyclopentane (**6i**) is tolerated from a potency perspective but negatively impacts the clearance, potentially due to the increased overall lipophilicity.

Reduction in the pK_a of the benzylic amine center (“pK_a2”) was attractive due to the potential to simultaneously impact P-gp efflux and hERG liabilities. Indeed, addition of an electron-withdrawing trifluoromethyl group onto the amine significantly improves both potency and ADME balance. Although the tertiary amine (**6j**) is much less potent in the WCA, the secondary amine (**6k**) retains good WCA potency and comparable LipE to the more basic analogues and exhibits enhanced BACE1 CFA potency and improved selectivity over BACE2 (5.8 \times vs 3.2 \times for **6f**). Although both CF₃ analogues have significantly improved MDR-based efflux ratios (1.7 and 1.2), the secondary amine **6k** shows greater metabolic stability (HLM CL_{int} = 12.0 mL/min/kg) than the methylated version **6j** (HLM = 29.4 mL/min/kg).

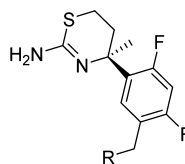
It was clear that the additional basic amine exerts a profound effect on whole-cell potency, reinforced by comparison to the previously described monocyclic analogue devoid of a P3 group (compound **6** in ref 21, BACE1 CFA IC₅₀ = 36 μ M, WCA IC₅₀ = 636 nM).²¹ The low molecular weight and dibasic nature of

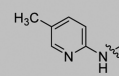
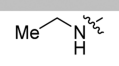
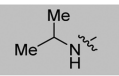
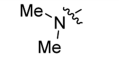
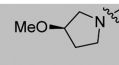
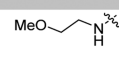
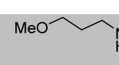
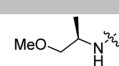
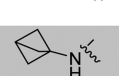
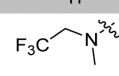
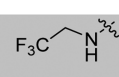
Scheme 1^a



^aReagents and conditions: (a) MeLi, Et₂O, *n*-BuLi, then DMF, -78 $^{\circ}$ C, 92%; (b) amine, Na(OAc)₃BH, DCE, rt, 22–97%; (c) HCl, dioxane, rt, 19–90%; (d) benzoic anhydride, TEA, THF/MeOH (2:1), rt, 86%; (e) N₂H₄·H₂O, EtOH, rt, 31%. P = Boc or benzoyl.

Table 1. In Vitro Data for 6a–k



Cpd	R =	BACE1 CFA IC ₅₀ (μM) ^a	BACE2 CFA IC ₅₀ (μM) ^b	CatD CFA IC ₅₀ (μM) ^c	BACE1 WCA IC ₅₀ (μM) ^d	MDR Er ^e	LogD	HLM ^f / (mL/m in/ kg)	WCA LE/LipE
6a		73.5	>100	>100	1.35 (54x)	8.8	2.4	199	0.34/ 5.2
6b		13.9	75.7	>100	0.008 (1,737x)	2.0	<-1.5	<8	0.57/ 9.9
6c		15.5	>94	>100	0.002 (7,750x)	ND	<-1.5	ND	0.58/ 10.2
6d		50.9	>100	>100	0.022 (2,313x)	ND	0.3	<8	0.54/ 7.6
6e		40.8	>100	>100	0.038 (1,073x)	7.9	0.4	17.4	0.44/ 7.3
6f		8.20	26.8	>100	0.006 (1,366x)	3.9	-0.3	<8	0.53/ 8.2
6g		35.1	62.9	>100	0.053 (1,186x)	9.0	-0.5	<8	0.45/ 8.1
6h		4.18	19.4	>100	0.004 (1,045x)	6.8	-0.3	<8	0.52/ 9.0
6i		2.10	17.5	95.3	0.004 (525x)	5.2	1.0	14.8	0.52/ 7.7
6j		20.2	>84	>100	1.013 (19.9x)	1.7	1.2	29.4	0.36/ 5.1
6k		1.31	7.6	>100	0.060 (21.8x)	1.2	1.0	12.0	0.45/ 6.7

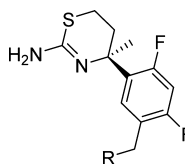
^aIC₅₀ values obtained from BACE1 CFA. ^bIC₅₀ values obtained from BACE2 CFA. ^cIC₅₀ values obtained from CatD CFA. ^dIC₅₀ values obtained from BACE1 WCA; value in parentheses is the BACE1 CFA/WCA ratio. ^eRatio from the MS-based quantification of apical/basal and basal/apical transfer rates of a test compound at 2 μM across contiguous monolayers from MDR1-transfected MDCK cells. ^fHepatic clearance predicted from in vitro human microsomal stability study.

the small alkyl exemplars result in highly ligand- and lipophilic efficient compounds in the whole-cell assay. While a similar rank order trend is observed for the BACE1 CFA, there is a 20–7750-fold disconnect observed between the two assay formats. This disconnect can be rationalized by the presence of the second basic center increasing the propensity for accumulation into the endosome, an acidic intracellular compartment where BACE1 is thought to be localized,³ in the WCA format. As expected, decreasing the basicity of the amine by the installation of an electron-withdrawing group significantly compresses the CFA/WCA disconnect.

It was recognized from the outset that the diversion from an amide moiety would likely result in a very different BACE1 substituent-derived SAR relative to the amides, as well as presenting distinct challenges to achieving a balanced ADME profile. A second round of amine optimization (Table 2) explored utilization of an electron-withdrawing group to balance ADME properties as well as incorporation of branched amines to further enhance potency. In an effort to more clearly

define the impact of the EWGs on ADME balance, we measured the pK_as for the amidine (“pK_a1”) and benzylic amine (“pK_a2”) for each of the analogues.²² Removal of one of the fluorines (6l) increases pK_a2 relative to analogue 6k, therefore increasing MDR Er (1.2 vs 3.1). Introduction of two geminal methyl groups provides a significant improvement in BACE1 CFA potency (6m vs 6k), albeit with a corresponding increase in MDR Er and a decrease in BACE2 selectivity (2 \times). Removal of one of the methyl groups (6n) decreases potency both in BACE1 CFA (1.9 μM) and WCA (64 nM) but improves efflux and BACE2 selectivity while reducing CYP 2D6 inhibition. Increasing the distance between the amine and trifluoromethyl groups (6o) increases pK_a2 and diminishes potency in both assay formats. In an effort to capitalize on the potency increase associated with increased substitution, cyclopropylamine-containing analogues (6p–q) were prepared. The cyclopropane unit is well tolerated, as exhibited by the excellent WCA potency, but suffers from a significant degradation in BACE1 CFA potency and MDR Er. The addition of a

Table 2. In Vitro Data for Compounds 6k–6u



Cpd	R =	BACE1 CFA IC ₅₀ (μ M) ^a	BACE2 CFA IC ₅₀ (μ M) ^b	CatD CFA IC ₅₀ (μ M) ^c	BACE 1 WCA IC ₅₀ (μ M) ^d	MDR Er ^e	LogD	HLM (mL/ min /kg) ^f	CYP 2D6 ^g	pK _a 1/ pK _a 2 ^h	hERG (μ M) ⁱ
6k		1.31	7.60	>100	0.060	1.2	1.0	12.0	25%	8.9/ 3.8	6.1
6l		5.89	27.3	>100	0.058	3.1	0.3	13.0	21%	8.9/ 5.2	14.7
6m		0.49	1.02	>100	0.031	3.6	1.5	<8.0	81%	8.9/ 4.2	11.2
6n		1.97	7.13	>100	0.064	2.2	0.6	11.9	45%	8.8/ 3.4	13.9
6o		54.7	>100	>100	0.400	6.1	0.5	9.3	39%	8.9/ 6.0	20.4
6p		20.6	>100	>100	0.030	3.4	0.5	<8.0	14%	9.0/ 6.2	49.2
6q		15.4	35.9	>100	0.014	6.9	0.1	<8	12%	9.3/ 6.3	33.0
6r		0.335	1.01	65.5	0.012	2.5	0.7	22.2	56%	8.8/ 4.2	13.7
6s		0.952	11.5	71.8	0.024	6.0	0.1	<8.0	40%	8.8/ 1.8	28.4
6t		0.770	1.89	>100	0.017	3.5	0.6	<8	45%	8.8/ NA	16.5
6u		0.069	0.405	32.4	0.018	1.5	1.8	<13	83%	9.0/ 2.9	3.5

^aIC₅₀ values obtained from BACE1 CFA. ^bIC₅₀ values obtained from BACE2 CFA. ^cIC₅₀ values obtained from CatD CFA. ^dIC₅₀ values obtained from BACE1 WCA. ^eRatio from the MS-based quantification of apical/basal and basal/apical transfer rates of a test compound at 2 μ M across contiguous monolayers from MDR1-transfected MDCK cells. ^fHepatic clearance predicted from in vitro human microsomal stability study. ^gCYP 2D6% inhibition determined in human microsomes using a probe CYP 2D6 substrate (dextromethorphan) and 3 μ M of test compound. ^hpK_a values measured. ⁱMeasured IC₅₀ in hERG-expressing CHO cells.

difluoromethyl group (**6r**) improves the BACE1 CFA potency and reduces the increase in MDR Er but simultaneously introduces a metabolic liability (HLM = 22 mL/min/kg). Replacement with a nitrile (**6s**) enhances BACE2 selectivity, but the MDR Er increases significantly (MDR Er = 6.0). Use of an oxetane (**6t**) in place of the cyclopropane improves WCA potency and decreases log *D* but results in an elevated MDR Er ratio (MDR Er = 3.5) nearly equivalent to that of the parent cyclopropylamine **6p**. In contrast, the CF₃-cyclopropyl derivative **6u** maintains good potency in both assay formats, exhibits a minimal efflux ratio and low clearance, and maintains excellent selectivity over CatD (470 \times) and modest selectivity over BACE2 (5.9 \times).

Although the decrease in pK_a2 imparted by the introduction of the cyclopropyl group in **6u** (2.9 vs 3.8 for **6k**) could

contribute to the improved BACE1 CFA potency, it is not sufficient to explain the 20-fold potency increase observed. To better rationalize this improvement, a co-crystal structure of compound **6u** in BACE1 was obtained (PDB: 5T1U). As shown in Figure 4, the thioamidine and difluorophenyl ring systems are oriented in a similar overall fashion to previously described BACE1 structures, with the difluorophenyl occupying the S1 pocket as expected. As predicted by our initial design hypothesis, the benzylic amine substituent adopts an orientation orthogonal to the plane of the difluorophenyl P1 group to optimally engage the carbonyl of Gly230. Interestingly, the trifluoromethyl group orients toward and fills the entrance to the S3 pocket, while the cyclopropyl substituent fills a small, lipophilic pocket at the back of the interface between the S1 and S3 pockets. Arguably, the significant

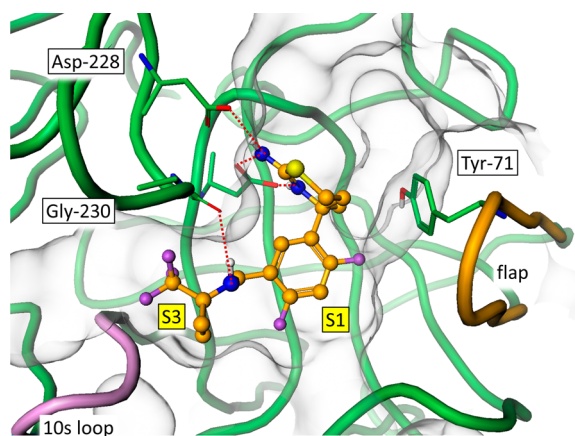


Figure 4. Crystal structure of **6u** in BACE1 binding site. PDB: 5T1U.

improvement in BACE1 CFA potency observed for **6u** is primarily achieved by optimally filling this cleft and locking the CF₃ into the direction of the S3 pocket.

Overall, a liability of the series is P-gp-mediated efflux, likely driven in large part by the presence of a third hydrogen bond donor and exacerbated by increasing basicity at the benzylic amine (**6o–6q**, $pK_a > 6$, MDR Er 3.4–6.9). It was recognized that the installation of an electron-withdrawing group at the amine center aids in overcoming this issue, as illustrated by the difluoromethyl-substituted analogue **6r**. Although the introduction of a nitrile substituent (**6s**) further lowers pK_a , the efflux liability increased, potentially because of the increase in polar surface area, a key factor for P-gp liability. In contrast, the relatively nonpolar trifluoromethyl group in **6u** decreases pK_a sufficiently, resulting in a decreased efflux ratio.

Gratifyingly, **6u** addresses a number of the key challenges that had emerged throughout the optimization of this series. As predicted by the in vitro transporter assay, **6u** exhibits free access to the CNS compartment in mice ($C_{u,b}/C_{u,p} = 1.0$), as determined by time-course AUC. To assess in vivo potency, analogue **6u** was dosed in wild-type mouse via subcutaneous administration at two doses, 10 and 100 mg/kg, to measure impact on levels of brain A β _{x-42}. At the lower dose, a small but significant decrease is observed at early time points, and at 100 mg/kg, robust lowering is observed out to 20 h postdose, providing a $C_{u,b}/C_{eff}$ of 31 nM for 25% A β lowering using previously described methodology (Figure 5).²³

A goal from the outset had been to mitigate the hERG liability often observed for BACE1 inhibitors. Therefore, hERG IC₅₀ values were generated for this second round of

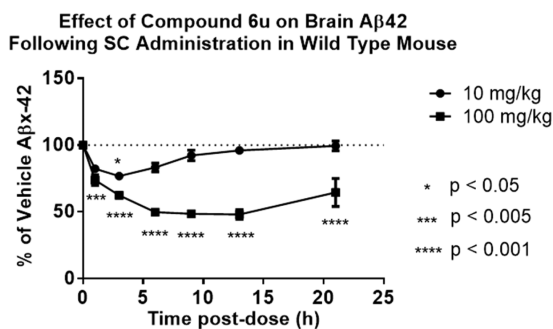


Figure 5. Effect of trifluoromethylcyclopropyl **6u** on brain A β _{x-42} following subcutaneous administration in wild-type mice.

optimization. All analogues exhibit some affinity for hERG (IC₅₀ 3.5–49 μ M), although there is no correlation with increasing log *D* and decreasing pK_a . The hERG TI, as defined by comparing the hERG IC₅₀ to the more robust and relevant measured $C_{u,p}/C_{eff}$ value for BACE1, provides the most appropriate selectivity descriptor; for **6u**, this corresponds to an in vivo hERG selectivity of 113 \times , satisfying our initial criteria.

Whereas **6u** had achieved a balance of A β -lowering in brain, CNS penetration, and selectivity over hERG, it was, unfortunately, also characterized by significant inhibition of cytochrome P450 subtype 2D6 (CYP 2D6). CYP inhibition, in general, is undesirable due to the potential for drug–drug interactions (DDI) through inhibition of oxidative metabolism, but the significance is enhanced for subtype 2D6 because of significant polymorphism in 2D6 expression.²⁴ Within this set of analogues, CYP 2D6 inhibition appears to be primarily driven by two main factors, namely, pK_a and the size of the benzylamine substituent. Unfortunately, the CYP 2D6 values inversely correlate to pK_a , such that analogues with decreased pK_a at the benzylic amine show greater inhibition, in direct opposition to the SAR utilized to obviate hERG and efflux transporter liabilities. In addition, increasing the size of the amine substituent appears to enhance CYP 2D6 inhibition, tracking with BACE1 potency. In an effort to more accurately gauge the CYP 2D6 inhibition, IC₅₀ curves were generated for a subset of these compounds. In this assay, the unflanked trifluoroethylamine **6k** showed only modest CYP 2D6 inhibition (IC₅₀ = 14 μ M), whereas **6u**, much more potent at BACE1, significantly inhibited CYP 2D6 (IC₅₀ = 157 nM). The intertwined SAR of CYP 2D6 inhibition, BACE1 potency, and transporter liability suggested that further tuning of the amine was unlikely to balance overall properties. Several alternative strategies were considered, including: (a) disrupting the favorable binding interactions between this series and CYP 2D6 while maintaining the high BACE1 affinity observed for **6u**, and (b) building upon the modest BACE1 potency and absence of CYP 2D6 liability associated with **6k**, but utilizing an alternative vector.

Disruption of the binding of this series to CYP 2D6 was informed by a recent report of a pyrazole-containing thioamidine series, which described a similar challenge with CYP 2D6 affinity (Figure 6).²⁵

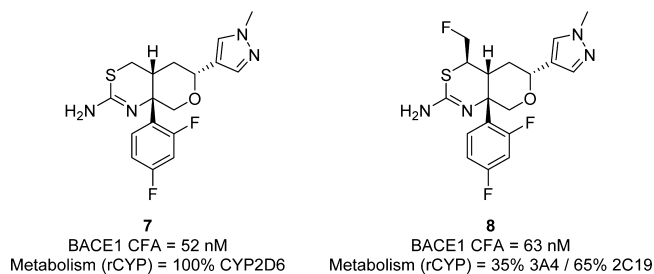
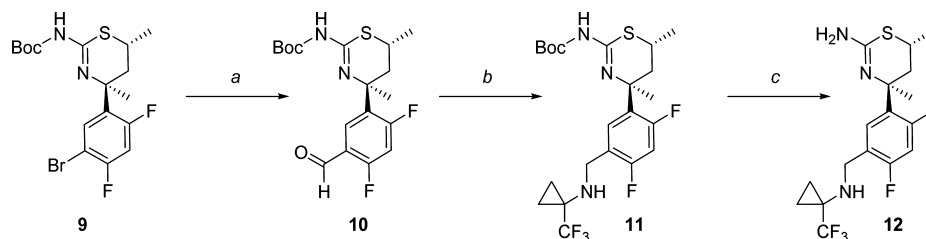


Figure 6. Metabolic profile of fused THP series.²⁵

In this case, the fused pyrazole **7** is metabolized exclusively by CYP 2D6. Additionally, the primary metabolism product observed, the demethylated pyrazole, is a potent inhibitor of CYP 2D6 (IC₅₀ = 0.37 μ M). The CYP 2D6 affinity in this series was ultimately conquered through the installation of a substituent [fluoromethyl (**8**) or methyl (not shown)] adjacent to sulfur that disrupts binding to the CYP 2D6 active site.

Scheme 2^a

^aReagents and conditions: (a) MeLi, Et₂O, *n*-BuLi, then DMF, -78 °C, 89%; (b) amine, Na(OAc)₃BH, DCE, rt, 93%; (c) HCl, dioxane, rt, 19%.

Table 3. In Vitro Profile of 12

compd	BACE1 CFA IC ₅₀ (μM) ^a	BACE2 CFA IC ₅₀ (μM) ^b	CatD CFA IC ₅₀ (μM) ^c	WCA IC ₅₀ (nM) ^d	MDR Er ^e	log <i>D</i>	HLM ^f (mL/min/kg)	CYP 2D6 IC ₅₀ (μM) ^g	pK _{a1} / pK _{a2}	hERG ^h (μM)
12	0.078	0.228	>100	0.024	3.2	2.4	38	0.334	8.8/2.8	2.6

^aIC₅₀ values obtained from BACE1 CFA assay. ^bIC₅₀ values obtained from BACE2 CFA assay. ^cIC₅₀ values obtained from CatD CFA assay. ^dIC₅₀ values obtained from BACE1 WCA. ^eRatio from the MS-based quantification of apical/basal and basal/apical transfer rates of a test compound at 2 μM across contiguous monolayers from MDR1-transfected MDCK cells. ^fHepatic clearance predicted from in vitro human microsomal stability study. ^gCYP 2D6 inhibition was obtained by measuring inhibition of 5 μM dextromorphan in pooled HLM (HL-MIX-102). ^hMeasured IC₅₀ in hERG-expressing CHO cells.

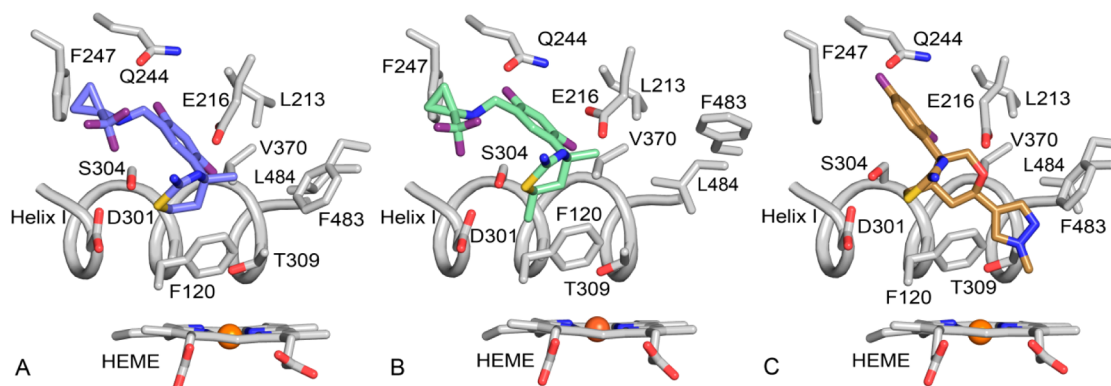


Figure 7. Comparison of the binding of 6u (A) and 12 (B) with the binding of 7 (C) in the active site of CYP 2D6.

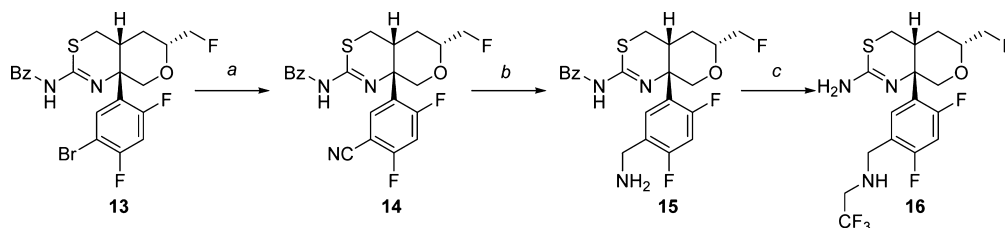
Utilization of this strategy guided the design of compound 12, where a chiral methyl group has been introduced next to the sulfur of the thioamidine (Scheme 2). This analogue was prepared in a similar fashion to the unsubstituted thioamidines, starting with the known bromide 9.²⁰

Overall, compound 12 maintains potency at BACE1 but exhibits increased clearance and MDR Er as compared to 6u (Table 3). These general trends were consistent with the pairwise changes associated with this matched molecular pair, as observed in the fused THP series. Interestingly, however, there was only modest impact on the CYP 2D6 inhibition (IC₅₀ = 334 nM) for this compound. The lack of translational impact for this methyl group across the two series is striking, and in an effort to better understand the inconsistent impact on CYP 2D6 inhibition, cocrystal structures of 6u and 12 in CYP 2D6 were generated.

X-ray crystal structures of CYP 2D6 with 6u and 12 bound were determined as described previously for 7²⁵ (PDB: 4XRY) by soaking crystals of a CYP 2D6 thioridazine complex with the appropriate compound (6u or 12). Comparison of the resulting structures (Figures 7A–C) illustrates that each of the thioamidines is anchored through an interaction with Glu-216, positioning the difluorophenyl ring proximal to helix I. The aminomethyl substituent in analogues 6u (Figure 7A) and 12 (Figure 7B) is oriented to the lipophilic pocket distal to the

heme, whereas the pyrazole of 7 is oriented toward the heme itself (Figure 7C). The orientations of the thioamidine rings in 6u and 12 are shifted, relative to that of the fused 7, to facilitate occupation of the distal pocket by the aminomethyl substituents. This reorientation creates greater distance between helix I and the difluorophenyl ring, and this shift is exacerbated slightly by the chiral methyl group in 12 (Figure 7B), which is easily accommodated. In contrast, the rigid architecture defined by the ring fusion of the thioamidine and THP restricts the rotation of 7 (Figure 7C), as the compound occupies the cleft between Phe-120 and the residues Glu-244 and Phe-247 on helix G. The addition of a methyl or fluoromethyl group next to the sulfur of 7 then creates a direct clash with helix I, as evidenced by the lack of affinity of 8. Therefore, this restricted rotation underlies the pronounced substituent impact on CYP 2D6 affinity in the fused series, whereas the facility for reorientation in the monocyclic series 6u/12 minimizes the substituent effect.

Therefore, an alternative strategy to mitigate CYP 2D6 affinity in the aminomethyl series would exploit the restricted rotation imparted by ring fusion, precluding occupation of the distal, lipophilic pocket of CYP 2D6 by an aminomethyl substituent. In addition, from experience in previous series, the fused THP ring would be expected to enhance BACE1 potency relative to the monocyclic congeners. Considering the increased

Scheme 3^a

^aReagents and conditions: (a) Pd₂(dba)₃, dppf, zinc, Zn(CN)₂, DMA, 130 °C, 85%; (b) Raney Ni, H₂, triethylamine, Boc₂O, H₂O, EtOH, rt, then HCl, MeOH, 61%; (c) 2,2,2-trifluoroethyl trifluoromethylsulfonate, trimethylamine, MeCN, 70 °C, then DBU, MeOH, 71%.

Table 4. In Vitro Data for Compound 16

compd	BACE1 CFA IC ₅₀ (μM) ^a	BACE2 CFA IC ₅₀ (μM) ^b	CatD CFA IC ₅₀ (μM) ^c	WCA IC ₅₀ (nM) ^d	MDR Er ^e	log D	HLM ^f (mL/min/kg)	CYP 2D6 IC ₅₀ (μM) ^g	pK _{a1} /pK _{a2}	hERG (μM) ^h	C _{u,b} / C _{u,p}	C _{eff} (C _{u,b} / nM)
16	0.077	0.295	>100	0.006	2.3	1.1	29	9.1	7.91/3.80	4.3	0.25	31

^aIC₅₀ values obtained from BACE1 CFA. ^bIC₅₀ values obtained from BACE2 CFA. ^cIC₅₀ values obtained from CatD CFA. ^dIC₅₀ values obtained from BACE1 WCA. ^eRatio from the MS-based quantification of apical/basal and basal/apical transfer rates of a test compound at 2 μM across contiguous monolayers from MDR1-transfected MDCK cells. ^fHepatic clearance predicted from in vitro human microsomal stability study. ^gCYP 2D6 inhibition was obtained by measuring inhibition of 5 μM dextromorphan in pooled HLM (HL-MIX-102). ^hMeasured IC₅₀ in hERG-expressing CHO cells.

lipophilicity and molecular weight imparted by bolting on the additional THP ring, the unflanked trifluoroethyl amine **6k** seemed an attractive starting template with which to execute this strategy. Fused analogue **16** was therefore designed and prepared as shown in Scheme 3. Starting from bromide **13**,²⁶ the aminomethyl linker was installed by Pd-mediated cyanation and subsequent reduction using Raney nickel. Alkylation of the resultant primary amine using trifluoroethyl triflate, followed by cleavage of the benzamide protecting group, provided the fused analogue **16**. The structure of **16** was confirmed by a single crystal X-ray structure carried out on the phosphate salt (see Supporting Information).

As expected, the bicyclic fusion offered a 17× improvement of BACE1 CFA potency for **16** relative to the monocyclic **6k** (Table 4), and **16** proved to be equipotent to **6u**, reinforcing the observation that potency can be obtained in either of the two available vectors. Further, **16** maintained excellent CatD selectivity, similar selectivity over BACE2 (3.8×) and a balanced overall ADME profile, including, gratifyingly, a significantly diminished CYP 2D6 liability (IC₅₀ = 9.1 μM, 118-fold selectivity over BACE1 CFA) relative to the monocyclic analogues. A modest increase in efflux was observed relative to **6k**, which translated into asymmetry in brain/plasma ratio (C_{u,b}/C_{u,p} = 0.25, AUC ratio). Additionally, **16** exhibited excellent central Aβ-lowering in mice, with a measured brain C_{eff} for 25% lowering of Aβ_{x-42} of 31 nM (Figure 8). The hERG value (IC₅₀ = 4.3 μM) was slightly improved relative to **6k**, reflecting a better nominal selectivity (139×). However, accounting for brain asymmetry, the resultant hERG TI diminishes to 35× over the requisite plasma concentrations.

The observation of such disparate responses in the relative affinities to BACE1 and CYP 2D6 for **16** versus **6k** was striking. The addition of the THP ring resulted in a 17× increase in potency at BACE1 while essentially having no impact on CYP 2D6 affinity (CYP 2D6 IC₅₀ for **6k** = 14 μM). A crystal structure of **16** in BACE1 was generated and confirmed that, as expected, reorganization of the S2' subpocket in BACE1 had occurred, driven by the rotation of Tyr71 to accommodate the THP ring and fluoromethyl substituent of **16** (Figure 9).

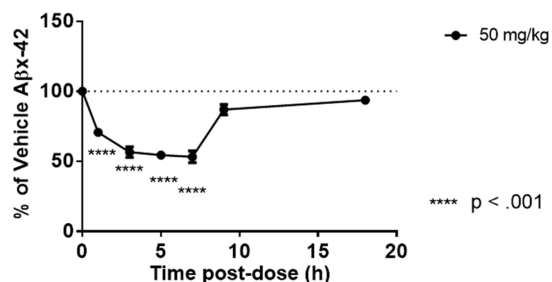
Effect of Compound 16 on Brain Aβ_{x-42} Following SC Administration in Wild Type Mouse

Figure 8. Effect of fused THP analogue **16** on brain Aβ_{x-42} following subcutaneous administration in wild-type mice.

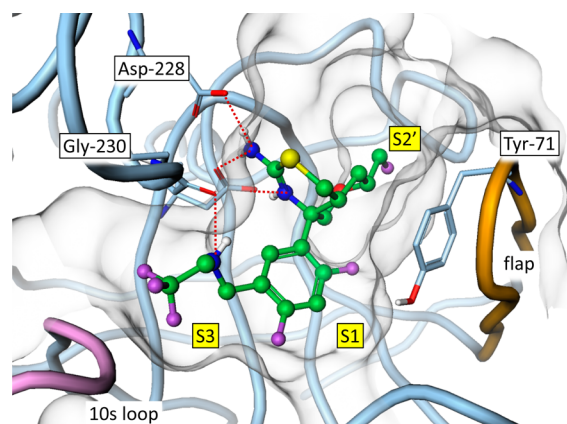


Figure 9. Co-crystal structure of **16** in BACE1. PDB: 5T1W.

Therefore, selectivity is realized because this subpocket in BACE1 is responsive to increases in lipophilic bulk in this vector, whereas the same vector in CYP 2D6 directs toward the heme and has no impact on affinity. In addition, the ring fusion limits the requisite rotation of the thioamidine ring to optimally accommodate the aminomethyl substituent within the CYP 2D6 binding site. This discrepant response contrasts with the

parallel responsiveness at BACE1 and CYP 2D6 for small changes in the benzylic amine of the monocyclic series, wherein equivalent increases in lipophilicity afforded corresponding enhancements in affinity for both BACE1 and CYP 2D6 receptors (**6k** vs **6u**, 20× BACE1, 9× CYP 2D6). Future BACE1 design efforts focused on avoiding CYP 2D6 liability will therefore target manipulation of the amidine “head group” architecture, rather than optimization of P3 substituents.

Upon the basis of its attractive balance of potency, selectivity, and CNS penetration, **16** was selected for further safety profiling. The compound showed excellent *in vitro* selectivity, as gauged by screening against the broad CEREP bioprint panel (<25% inhibition at all targets at 10 μ M). Subsequent advancement to long-term *in vivo* toxicology studies, including a 4-week arm at 100 mg/kg (30× AUC over C_{eff}), revealed no ocular findings, presumably reflecting the excellent *in vitro* selectivity observed for **16**.

CONCLUSION

The optimization of a series of brain-penetrant BACE1 inhibitors with a novel aminomethyl linker has been described. This linker mitigates an aniline structural alert prevalent throughout a large contingent of literature BACE1 series. Careful modulation of the amine substituent aided in garnering a balanced profile, as the inherent efflux transporter liability and potency are dependent upon the resultant pK_a . A number of the more active compounds carried significant CYP 2D6 inhibition that correlated well with the size of the amine substituent. Unlike the fused THP series, substitution on the monocyclic thioamidine ring did not ameliorate CYP 2D6 inhibition, which was rationalized through examination of CYP 2D6 crystal structures. Filling the BACE1 S2' subpocket by fusing a THP ring onto the monocyclic thioamidine ring improved BACE1 potency dramatically without impacting CYP 2D6 affinity. One such example (**16**) demonstrates good ADME balance, modest brain asymmetry, no DDI potential, and good *in vivo* efficacy, illustrating that the aminomethyl linker can serve as a robust replacement to overcome the significant challenges and structural alerts inherent in the classical P1/P3 amide of previously described BACE1 inhibitors.

EXPERIMENTAL SECTION

Biology. *In Vitro* Pharmacology. sAPP β Whole-Cell Assay (WCA). sAPP β , the primary cleavage product of BACE1, was determined in H4 human neuroglioma cells overexpressing the wild-type human APP₆₉₅. Cells were treated for 18 h with compound in a final concentration of 1% DMSO. sAPP β levels were measured by ELISA with a capture APP N-terminal antibody (Affinity BioReagents, OMA1-03132), wild-type sAPP β -specific reporter antibody p192 (Elan), and tertiary antirabbit-HRP (GE Healthcare). The colorimetric reaction was read by an EnVision (PerkinElmer) plate reader.

BACE1 Enzyme Cell-Free Assay (FP). Beta secretase-1 activity was assessed with soluble BACE1 and the synthetic APP substrate Biotin-GLTNIKTEEISEISYEVEFR-C[oregon green]KK-OH in the presence of compounds in a fluorescence polarization (FP) *in vitro* assay. Enzyme, substrate and test compounds were incubated in 15 μ L of 100 mM sodium acetate pH = 4.5 buffer containing 0.001% Tween-20 for 3 h at 37 °C. Following the addition of saturating immunopure streptavidin, fluorescence polarization was measured with a PerkinElmer EnVision plate reader (Ex485 nm/Em530 nm).

***In Vivo* Experiments.** All procedures performed on animals in this study were in accordance with established guidelines and regulations, and were reviewed and approved by the Pfizer (or other) Institutional Animal Care and Use Committee. Pfizer animal care facilities that supported this work are fully accredited by AAALAC International.

Acute Treatment in Mice. Male 129/SVE wild-type mice (20–25 g) were in a nonfasted state prior to subcutaneous dosing with vehicle, or compound **6u** or **16**, using a dosing volume of 10 mL/kg in 5:5:90 DMSO:cremophor:saline vehicle. Mice ($n = 5$ per group) were sacrificed at 1, 3, 5, 7, 14, 20, and 30 h postdose. Whole blood samples (0.5–1.0 mL) were collected by cardiac puncture into ethylenediaminetetraacetic acid (EDTA)-containing tubes, and plasma was separated by centrifugation (1500g for 10 min at 4 °C). The generated plasma was distributed into separate tubes on wet ice for exposure measurements (50 μ L) and A β analysis (remainder). CSF samples (8–12 μ L) were obtained by cisterna magna puncture using a sterile 25 gauge needle and collected with a P-20 Eppendorf pipet. CSF samples were distributed into separate tubes on dry ice for exposure measurements (3 μ L) and A β analysis (remainder). Whole brain was removed and divided for exposure measurements (cerebellum) and A β analysis (left and right hemispheres), weighed, and frozen on dry ice. All samples were stored at –80 °C prior to assay.

Measurement of Rodent Amyloid- β . Frozen mouse hemibrains were homogenized (10% w/v) in 5 M guanidine HCl, using a Qiagen TissueLyser. Each sample was homogenized with a 5 mm stainless steel bead, four times, at a shaking rate of 24 times/s for 90 s, then incubated at 25 °C for 3 h, and ultracentrifuged at 125000g for 1 h at 4 °C. The resulting supernatant was removed and stored in a 96-well polypropylene deep well plate at –80 °C. The A β peptides were further purified through solid-phase extraction using Waters Oasis reversed-phase HLB 96-well column plates (60 mg). Column eluates in ammonium hydroxide from 500 to 800 μ L of original brain supernatant were evaporated to complete dryness and stored at –80 °C until assay. For plasma analysis, 140–175 μ L of mouse plasma was treated 1:1 with 5 M guanidine HCl and incubated overnight with rotation at 4 °C. The entire volume was then purified through solid-phase extraction as indicated above.

Samples were analyzed using a Dissociation-Enhanced Lanthanide Fluorescent Immunoassay (DELFLIA) platform Enzyme-Linked Immunosorbent Assay (ELISA). Configuration of the antibodies used in determining the level of A β x-40 and A β x-42 utilizes a common detect antibody (4G8) in combination with specific C-terminal antibodies for the 40 and 42 cleavage sites. For the A β x-40 assay, a 384-well black Nunc Maxisorp plate was coated with 15 μ L/well (4 μ g/mL) capture antibody (Rinat 1219) in 0.1 M sodium bicarbonate coating buffer, pH 8.2. For the A β x-42 assay, 15 μ L/well (8 μ g/mL) capture antibody (Rinat 10G3) was used. The plates were sealed and incubated at 4 °C overnight. Plates were washed with phosphate-buffered saline containing 0.05% Tween-20 (PBS-T) and blocked with 75 μ L of blocking buffer (1% BSA in PBS-T) for 2 h at 25 °C.

After washing the plates with PBS-T, rodent A β x-40 (California Peptide) or A β x-42 (California Peptide) standard was serially diluted in blocking buffer and 15 μ L was applied to the plate in quadruplicate. Dried brain samples were reconstituted in 120 μ L of blocking buffer, which corresponds to a 4.16–6.67-fold concentration. Then 15 μ L of undiluted brain sample was added to the A β x-42 assay plate in triplicate or 15 μ L of a 1:2 diluted brain sample was added to the A β x-40 assay plate in triplicate. Dried plasma samples were reconstituted in 40 μ L of blocking buffer, which corresponds to a 3.5–4.38-fold concentration, and 15 μ L was added to the A β x-40 assay plate in duplicate. CSF samples were diluted 1:8 in blocking buffer, and 15 μ L was added to the A β x-40 assay plate in duplicate. Plates were incubated with sample or standards for 2 h at 25 °C. The plates were washed with PBS-T, and 15 μ L of detecting antibody (4G8-Biotin, Covance), 200 ng/mL in blocking buffer, was added to each well, incubating for 2 h at 25 °C. The plates were then washed with PBS-T, and 15 μ L of europium-labeled streptavidin (PerkinElmer), 50 ng/mL in blocking buffer, was added for a 1 h incubation in the dark at 25 °C. The plates were washed with PBS-T, and 15 μ L of PerkinElmer Enhancement solution was added to each well with 20 min incubation at rt. Plates were read on an EnVision plate reader using DELFLIA time-resolved fluorimetry (Exc340/Em615), and samples were extrapolated against the standard curve using four-parameter logistics. Measurement of human amyloid- β in plasma and CSF from PS1/APP

mice utilizes the same capture and detecting antibodies used for wild-type mice. Vehicle-treated samples from plasma and CSF were serially diluted to optimize sample dilution to the linear phase of an $A\beta$ peptide standard curve. $A\beta$ levels were measured using DELFIA ELISA.

Neuropharmacokinetic Studies in Male CD-1 Mice. The in-life and bioanalytical portions of these studies were conducted at BioDuro, Pharmaceutical Product Development Inc. (Beijing, China). Male CD-1 mice were obtained from PUMC, China. Mice received a 10 mg/kg subcutaneous (sc) dose of compounds **6u** or **16**. The doses were prepared in 5% DMSO/95% water containing (v/v) 0.5% methylcellulose (w/v) and delivered in a volume of 5 mL/kg. Animals were sacrificed in a CO₂ chamber. Blood, brain, and CSF samples were collected at 1, 4, and 7 h postdosing. Plasma was isolated after centrifugation. The plasma, brain, and CSF samples were stored at $-80\text{ }^{\circ}\text{C}$ prior to analysis.

Measurement of Fractions Unbound in Brain. The unbound fraction of each compound was determined in brain tissue homogenate using a 96-well equilibrium dialysis method as described by Kalvass et al.²⁷ with the following exceptions. Brain homogenates were prepared from freshly harvested rat brains following dilution with a 4-fold volume of phosphate buffer and spiked with 1 μM compound. The homogenates were dialyzed against an equal volume (150 μL) of phosphate buffer at $37\text{ }^{\circ}\text{C}$ for 6 h. Following the incubation, equal volumes (50 μL) of brain homogenate and buffer samples were collected and mixed with 50 μL of buffer or control homogenate, respectively, for preparation of mixed matrix samples. All samples were then precipitated with internal standard in acetonitrile (200 μL), vortexed, and centrifuged. Supernatants were analyzed using an LC-MS/MS assay. A dilution factor of 5 was applied to the calculation of brain fraction unbound.

Generic Liquid Chromatography Tandem Mass Spectrometry (LC-MS/MS) Assay for Exposure Measurements in Plasma, Brain, and CSF. Plasma, brain, and CSF were collected as described above and frozen at $-80\text{ }^{\circ}\text{C}$ until analysis by LC-MS/MS. Standard curves were prepared in respective matrix via serial dilution at a concentration of 1.0–2000 ng/mL (plasma and CSF) or 0.5–2000 ng/g (brain). For plasma, a 50 mL aliquot of sample was precipitated with 500 mL of MTBE containing an internal standard. Samples were vortexed for 1 min, then centrifuged at 3000 rpm for 10 min. The supernatant was transferred to a 96-well plate. Frozen brain tissue was weighed, and an 2-propanol:water (60:40) volume equivalent to 4 times the mass was added before homogenization in a bead beater (BioSpec Products Inc., Bartlesville, OK). A 50 mL aliquot of sample was precipitated with 500 mL of MTBE containing an internal standard. Samples were vortexed for 1 min, then centrifuged at 3000 rpm for 10 min. The supernatant was transferred to a 96-well plate. For CSF, a 50 mL aliquot of sample was precipitated with 500 mL of MTBE containing an internal standard. Samples were vortexed for 1 min, then centrifuged at 3000 rpm for 10 min. The supernatant (300 mL) was transferred to a 96-well plate. LC-MS/MS analysis was carried out using a high-performance liquid chromatography system consisting of tertiary Shimadzu LC20AD pumps (Shimadzu Scientific Instruments, Columbia, MD) with a CTC PAL autosampler (Leap Technologies, Carrboro, NC) interfaced to an API 4000 LC-MS/MS quadrupole tandem mass spectrometer (AB Sciex Inc., Ontario, Canada). The mobile phase consisted of solvent A (water with 0.1% formic acid) and solvent B (acetonitrile with 0.1% formic acid). The gradient was as follows: solvent B was held at 5% for 0.4 min, linearly ramped from 5% to 95% in 0.5 min, held at 95% for 0.6 min, and then stepped to 5% over 0.01 min. The mass spectrometer was operated using positive electrospray ionization. All raw data was processed using Analyst Software version 1.4.2 (AB Sciex Inc., Ontario, Canada).

hERG Patch Clamp Assay. All testing was carried out in CHO cells transfected with the hERG gene, purchased from Millipore (PrecisION hERG-CHO Recombinant Cell Line CYL3038). The cell line was grown in DMEM/F-12, GlutaMAX with 10% fetal bovine serum, 1% penicillin–streptomycin, 1% geneticin, and 1% of 1 M HEPES buffer solution, and maintained at approximately $37\text{ }^{\circ}\text{C}$ in a humidified atmosphere containing 5% carbon dioxide. The cells were

passed every 3–5 days based on confluency. On the day of the experiment, 50%–80% confluent cells were harvested from a 175 cm² culture flask using Detachin. After 10 min of exposure to Detachin at $37\text{ }^{\circ}\text{C}$, the cells were centrifuged for 1 min at 1000 rpm. The supernatant was removed, and the cell pellet was reconstituted in 5–8 mL of serum-free media with 2.5% of 1 M HEPES, placed on the Qstirrer, and allowed to recover. After a ~ 30 min recovery period, experiments were initiated.

hERG Potassium Channel Current Recordings. hERG current was elicited and recorded using the automated Qpatch HT system.²⁸ The suspended cells in the Qstirrer were transferred to 48 individual recording chambers on a Qplate 48 containing extracellular recording saline composed of (in mM): 132 NaCl, 4 KCl, 1.8 CaCl₂, 1.2 MgCl₂, 10 HEPES, 11.1 glucose, and adjusted to pH 7.35 ± 0.1 with NaOH. The intracellular recording saline was composed of (in mM): 70 KF, 60 KCl, 15 NaCl, 5 EGTA, 5 HEPES, and adjusted to pH 7.2 ± 0.1 with KOH. Membrane currents were recorded at room temperature.

hERG current was elicited from a holding potential of -80 mV with a voltage step to $+30$ mV for 1 s, followed by a ramp back to -80 mV at 0.55 mV/ms. Test pulses were delivered at a frequency of 0.25 Hz. Up to four different concentrations were studied for each cell, each exposure lasting 5 min or until steady-state effects were observed. In a separate set of experiments, full concentration–response relationships were determined for the positive control, cisapride, and an IC₅₀ was reported for this study.

hERG Data Analysis. Using Sophion Qpatch Assay Software, the amplitude of the peak outward hERG current upon repolarizing ramp was measured. Current amplitude was determined by taking the average of the last five current peaks under each treatment condition. Percent inhibition was determined by taking the ratio of the current measured at steady state in the presence of test article ($I_{\text{test article}}$) versus the control current (I_{control}) and expressed as % inhibition = $100 - (I_{\text{test article}}/I_{\text{control}}) \times 100$. When possible, a concentration–response curve was plotted and the data were fitted using Qpatch software to determine an IC₅₀. The $P < 0.05$ was considered statistically significant. Data were presented as mean \pm SEM.

Crystallization of BACE. Crystals of BACE were prepared as previously described,²⁹ with several modifications to the protein purification scheme. Ni²⁺ affinity and size exclusion chromatography were used as the initial purification steps yielding homogeneous BACE and eliminating the need for a peptide affinity column. Following removal of the prodomain by furin (0.0375 U/mg BACE), anion exchange chromatography (GE Healthcare 1 mL of Q HP) was used as a final purification step. Compounds **6u** and **16** were soaked into crystals grown using the procedure described in ref 21. The crystals were soaked at 0.6 mM for 3 h, transferred to a cryoprotectant comprised of 80% mother liquor/20% glycerol, and subsequently flash cooled in liquid nitrogen. X-ray diffraction data for compound **6u** was collected at sector 17ID at the Advanced Photon Source (Argonne National Laboratory, Argonne, IL, USA) on a Pilatus 6 M detector at $-170\text{ }^{\circ}\text{C}$. Data for compound **16** was collected in-house on a Rigaku FRE rotating anode X-ray generator equipped with a Rigaku Saturn 944 CCD detector. All data was processed using AUTOPROC³⁰ and XDS,³¹ and subsequent data manipulation was performed using the CCP4 suite of programs.³² Initial structures were determined by rigid body refinement of a reference BACE structure, followed by restrained positional refinement in REFMAC.³³ Ligands were automatically fit to difference maps calculated after refinement in AUTOBUSTER,³⁴ and all further refinement was performed in AUTOBUSTER. Data and refinement statistics are reported in Table S1 (see Supporting Information).

Crystallization of CYP 2D6. Structural characterization of the binding of **6u** and **12** to CYP 2D6 was determined by X-ray crystallography (PDB: 5TFT and 5TFU, respectively). Crystals of a CYP 2D6 thioridazine complex were prepared and soaked with an artificial mother liquor containing each of the compounds, with repeated transfers to fresh mother liquor to exchange the thioridazine for the new compound as described previously.²⁵ Stock solutions (10 \times) were prepared in DMSO, and the final concentration of each compound in the artificial mother liquor was 5 mM. Data sets were

collected at the Stanford Synchrotron Light Source from single crystals at a temperature of 100 K. The data were integrated with XDS³¹ and merged, scaled, and processed using the CCP4 suite of programs.³² As the space group and unit cell were highly similar to that used to determine PDB 4XRY, molecular replacement by rigid body refinement was used for the four chains of the 4XRY structure. Model building and refinement employed COOT³⁵ and Phenix 1.9,³⁶ respectively. The data processing and model refinement statistics are provided in Supporting Information, Table S2.

Chemistry. General Methods. Solvents and reagents were of reagent grade and were used as supplied by the manufacturer. All reactions were run under a N₂ atmosphere. Organic extracts were routinely dried over anhydrous Na₂SO₄. Concentration refers to rotary evaporation under reduced pressure. Chromatography refers to flash chromatography using disposable RediSepRf 4–120 g silica columns or Biotage disposable columns on a CombiFlash Companion or Biotage Horizon automatic purification system. Microwave reactions were carried out in a SmithCreator microwave reactor from Personal Chemistry. Purification by mass-triggered HPLC was carried out using Waters XTerra PrepMS C18 columns, 5 μm, 30 mm × 100 mm. Compounds were presalted as TFA salts and diluted with 1 mL of dimethyl sulfoxide. Samples were purified by mass-triggered collection using a mobile phase of 0.1% trifluoroacetic acid in water and acetonitrile with a gradient of 100% aqueous to 100% acetonitrile over 10 min at a flow rate of 20 mL/min. Elemental analyses were performed by QTI, Whitehouse, NJ. All target compounds were analyzed using ultra high performance liquid chromatography/ultraviolet/evaporative light scattering detection coupled to time-of-flight mass spectrometry (UHPLC/UV/ELSD/TOFMS). Unless otherwise noted, all tested compounds were found to be >95% pure by this method. Each of the amine fragments employed in the reductive amination to prepare 6a–u has been previously described in the literature.

UHPLC/MS Analysis. The UHPLC was performed on a Waters ACQUITY UHPLC system (Waters, Milford, MA), which was equipped with a binary solvent delivery manager, column manager, and sample manager coupled to ELSD and UV detectors (Waters, Milford, MA). Detection was performed on a Waters LCT premier XE mass spectrometer (Waters, Milford, MA). The instrument was fitted with an Acquity Bridged Ethane Hybrid (BEH) C18 column (30 mm × 2.1 mm, 1.7 μm particle size, Waters, Milford, MA) operated at 60 °C.

tert-Butyl (S)-4-(2,4-Difluoro-5-formylphenyl)-4-methyl-5,6-dihydro-4H-1,3-thiazin-2-yl)carbamate (4). To a cooled solution (–78 °C) of 3 (2.61 g, 6.17 mmol) in anhydrous ether (61.7 mL) was added methylolithium (4.44 mL, 7.10 mmol) dropwise. The mixture was stirred for 30 min before *n*-BuLi (3.2 mL, 8.64 mmol) was added dropwise at –78 °C. The reaction mixture was stirred for another 30 min before the addition of DMF (4.78 mL, 61.7 mmol) in one portion. The reaction was stirred for 1 h and slowly warmed up to –20 °C, then quenched with aq NH₄Cl (50 mL). The layers were separated, and the aqueous layer was extracted with EtOAc (2×). The combined organic layers were washed with brine (1×), dried (Na₂SO₄), concentrated, and purified by silica chromatography using a 0–40% EtOAc/heptane gradient to yield the product as a colorless solid. Yield: 92%. LCMS *m/z* 371.4 [M – H⁺]. ¹H NMR (400 MHz, CDCl₃) δ 10.27 (s, 1H), 7.87–8.00 (m, 1H), 6.88–7.01 (m, 1H), 2.90–3.02 (m, 1H), 2.75–2.87 (m, 1H), 2.62–2.71 (m, 1H), 2.11–2.21 (m, 1H), 1.68 (br s, 3H), 1.48–1.58 (m, 9H).

tert-Butyl (S)-4-(2,4-Difluoro-5-((5-methylpyridin-2-yl)amino)methyl)phenyl)-4-methyl-5,6-dihydro-4H-1,3-thiazin-2-yl)carbamate (5a). To a solution of 4 (75 mg, 0.20 mmol) in dichloroethane (0.68 mL, 0.2 M) was added 5-methylpyridin-2-amine (33 mg, 0.30 mmol, 1.5 equiv) and Na(OAc)₃BH (84 mg, 0.40 mmol, 2 equiv). The resulting solution was stirred for 2 h at rt. The reaction mixture was then partitioned between aq NaHCO₃ and CH₂Cl₂. The organic layer was separated, and the aq layer was back-extracted with CH₂Cl₂ (2×). The combined organics were then washed with brine (1×), dried over Na₂SO₄, concentrated, and purified by silica chromatography (4 g silica column, using a 10–100% EtOAc/heptane

gradient) to afford a colorless oil in 60% yield. LCMS *m/z* 463.4 [M – H⁺]. ¹H NMR (400 MHz, CDCl₃) δ 7.88–7.95 (m, *J* = 1.6 Hz, 1H), 7.36 (t, *J* = 8.8 Hz, 1H), 7.25 (dd, *J* = 2.2, 8.4 Hz, 1H), 6.83 (dd, *J* = 9.4, 11.7 Hz, 1H), 6.37 (d, *J* = 8.2 Hz, 1H), 4.75–4.92 (m, 1H), 4.44–4.58 (m, 2H), 2.74–2.84 (m, 1H), 2.65–2.74 (m, 1H), 2.55 (dt, *J* = 12.3, 3.1 Hz, 1H), 2.18 (s, 3H), 1.97–2.10 (m, 1H), 1.69 (s, 3H), 1.53 (s, 9H).

tert-Butyl (S)-4-(5-((Ethylamino)methyl)-2,4-difluorophenyl)-4-methyl-5,6-dihydro-4H-1,3-thiazin-2-yl)carbamate (5b). The title compound was prepared from 4 (150 mg, 0.405 mmol) and ethanamine (27 mg, 0.61 mmol) according to a similar procedure as for the preparation of 5a in 88% yield. LCMS *m/z* 400.4 [M – H⁺]. ¹H NMR (400 MHz, CDCl₃) δ 7.18–7.27 (m, 1H), 6.81 (dd, *J* = 11.7, 9.4 Hz, 1H), 3.71–3.85 (m, 2H), 2.77–2.86 (m, 1H), 2.69–2.77 (m, 1H), 2.65 (q, *J* = 7.0 Hz, 2H), 2.51–2.60 (m, 1H), 1.98–2.09 (m, 2H), 1.70 (s, 3H), 1.50 (s, 9H), 1.11 (t, *J* = 7.2 Hz, 3H).

tert-Butyl (S)-4-(2,4-Difluoro-5-((isopropylamino)methyl)phenyl)-4-methyl-5,6-dihydro-4H-1,3-thiazin-2-yl)carbamate (5c). The title compound was prepared from 4 (50 mg, 0.13 mmol) and propan-2-amine (12 mg, 0.20 mmol, 1.5 equiv) according to a similar procedure as for the preparation of 5a in 61% yield. LCMS *m/z* 414.4 [M – H⁺]. ¹H NMR (400 MHz, CDCl₃) δ 7.28–7.35 (m, 1H), 6.83 (dd, *J* = 11.7, 9.4 Hz, 1H), 3.77–3.90 (m, 2H), 2.78–2.89 (m, 2H), 2.66–2.75 (m, 1H), 2.60 (dt, *J* = 12.3, 3.1 Hz, 1H), 2.02–2.12 (m, 1H), 1.70 (s, 3H), 1.52 (s, 9H), 1.13 (d, *J* = 6.2 Hz, 6H).

tert-Butyl (S)-4-(5-((Dimethylamino)methyl)-2,4-difluorophenyl)-4-methyl-5,6-dihydro-4H-1,3-thiazin-2-yl)carbamate (5d). The title compound was prepared from 4 (78 mg, 0.21 mmol) and dimethylamine (158 μL, 0.32 mmol, 2 M in methanol) according to a similar procedure as for the preparation of 5a in 59% yield. LCMS *m/z* 400.4 [M – H⁺]. ¹H NMR (400 MHz, CDCl₃) δ 7.25 (t, *J* = 8.8 Hz, 1H), 6.82 (dd, *J* = 11.9, 9.2 Hz, 1H), 3.39–3.54 (m, 2H), 2.79–2.89 (m, 1H), 2.67–2.77 (m, 1H), 2.59 (dt, *J* = 12.3, 3.1 Hz, 1H), 2.23 (s, 6H), 2.03–2.12 (m, 1H), 1.71 (s, 3H), 1.50 (s, 9H).

tert-Butyl ((S)-4-(2,4-Difluoro-5-(((R)-3-methoxyprolidin-1-yl)methyl)phenyl)-4-methyl-5,6-dihydro-4H-1,3-thiazin-2-yl)carbamate (5e). The title compound was prepared from 4 (160 mg, 0.43 mmol) and (R)-3-methoxyprolidine (66 mg, 0.65 mmol) according to a similar procedure as for the preparation of 5a in 59% yield. LCMS *m/z* 456.4 [M – H⁺]. ¹H NMR (400 MHz, CDCl₃) δ 7.27 (t, *J* = 8.59 Hz, 1H), 6.80 (dd, *J* = 8.98, 11.71 Hz, 1H), 3.86–3.96 (m, 1H), 3.57–3.73 (m, 2H), 3.25 (s, 3H), 2.78–2.91 (m, 2H), 2.70–2.78 (m, 1H), 2.59–2.70 (m, 1H), 2.50–2.59 (m, 2H), 2.46 (dd, *J* = 9.9, 3.7 Hz, 1H), 1.96–2.11 (m, 2H), 1.73–1.82 (m, 1H), 1.71 (s, 3H), 1.51 (s, 9H).

tert-Butyl (S)-4-(2,4-Difluoro-5-(((2-methoxyethyl)amino)methyl)phenyl)-4-methyl-5,6-dihydro-4H-1,3-thiazin-2-yl)carbamate (5f). The title compound was prepared from 4 (115 mg, 0.31 mmol) and 2-methoxyethan-1-amine (35 mg, 0.47 mmol) according to a similar procedure as for the preparation of 5a in 72% yield. LCMS *m/z* 430.5 [M – H⁺]. ¹H NMR (400 MHz, CDCl₃) δ 7.21–7.33 (m, 1H), 6.82 (dd, *J* = 9.17, 11.90 Hz, 1H), 3.75–3.88 (m, 2H), 3.50 (t, *J* = 5.1 Hz, 2H), 3.30–3.39 (m, 3H), 2.69–2.88 (m, 4H), 2.59 (dt, *J* = 12.3, 3.1 Hz, 1H), 1.98–2.10 (m, 2H), 1.71 (s, 3H), 1.52 (s, 9H).

tert-Butyl (S)-4-(2,4-Difluoro-5-(((3-methoxypropyl)amino)methyl)phenyl)-4-methyl-5,6-dihydro-4H-1,3-thiazin-2-yl)carbamate (5g). The title compound was prepared from 4 (95 mg, 0.26 mmol) and 3-methoxypropan-1-amine (34 mg, 0.38 mmol) according to a similar procedure as for the preparation of 5a in 58% yield. LCMS *m/z* 444.4 [M – H⁺]. ¹H NMR (400 MHz, CDCl₃) δ 7.25 (t, *J* = 8.7 Hz, 1H), 6.80 (dd, *J* = 11.7, 9.2 Hz, 1H), 3.74–3.84 (m, 2H), 3.43 (t, *J* = 6.0 Hz, 2H), 3.28–3.31 (m, 3H), 2.78–2.84 (m, 1H), 2.70 (t, *J* = 6.8 Hz, 3H), 2.53–2.62 (m, 1H), 1.99–2.08 (m, 1H), 1.76 (quin, *J* = 6.5 Hz, 2H), 1.69 (s, 3H), 1.49 (s, 9H).

tert-Butyl ((S)-4-(2,4-Difluoro-5-(((R)-1-methoxypropan-2-yl)amino)methyl)phenyl)-4-methyl-5,6-dihydro-4H-1,3-thiazin-2-yl)carbamate (5h). The title compound was prepared from 4 (120 mg, 0.32 mmol) and the HCl salt of (R)-1-methoxypropan-2-amine (61 mg, 0.49 mmol) according to a similar procedure as for the preparation of 5a in 68% yield. LCMS *m/z* 444.4 [M – H⁺]. ¹H

NMR (400 MHz, CDCl₃) δ 7.22–7.31 (m, 1H), 6.80 (dd, J = 9.37, 11.71 Hz, 1H), 3.80 (s, 2H), 3.25–3.37 (m, 4H), 3.17–3.25 (m, 1H), 2.69–2.93 (m, 3H), 2.57 (dt, J = 12.2, 2.9 Hz, 1H), 1.96–2.10 (m, 1H), 1.69 (s, 3H), 1.50 (s, 9H), 1.03 (d, J = 6.2 Hz, 3H).

tert-Butyl (S)-4-(5-((Bicyclo[1.1.1]pentan-1-ylamino)methyl)-2,4-difluorophenyl)-4-methyl-5,6-dihydro-4H-1,3-thiazin-2-yl)-carbamate (5i). The title compound was prepared from 4 (100 mg, 0.27 mmol) and bicyclo[1.1.1]pentan-1-amine (34 mg, 0.40 mmol) according to a similar procedure as for the preparation of 5a in 31% yield. LCMS m/z 438.4 [M – H⁺]. ¹H NMR (400 MHz, CDCl₃) δ 7.23–7.34 (m, 1H), 6.82 (dd, J = 11.7, 9.4 Hz, 1H), 3.73–3.87 (m, 2H), 2.73–2.90 (m, 2H), 2.52–2.68 (m, 1H), 2.02–2.12 (m, 1H), 1.75–1.81 (m, 5H), 1.72 (s, 3H), 1.54 (s, 9H), 1.20–1.35 (m, 2H).

tert-Butyl (S)-4-(2,4-Difluoro-5-((methyl(2,2,2-trifluoroethyl)amino)methyl)phenyl)-4-methyl-5,6-dihydro-4H-1,3-thiazin-2-yl)-carbamate (5j). The title compound was prepared from 4 (165 mg, 0.44 mmol) and the HCl salt of 2,2,2-trifluoro-*N*-methylethan-1-amine (100 mg, 0.67 mmol) according to a similar procedure as for the preparation of 5a in 22% yield. LCMS m/z 468.3 [M – H⁺]. ¹H NMR (400 MHz, CDCl₃) δ 7.32 (t, J = 8.8 Hz, 1H), 6.84 (dd, J = 11.7, 9.0 Hz, 1H), 3.76 (s, 2H), 3.06 (q, J = 9.4 Hz, 2H), 2.80–2.88 (m, 1H), 2.69–2.80 (m, 1H), 2.58 (dt, J = 12.4, 3.3 Hz, 1H), 2.43 (s, 3H), 2.07 (dt, J = 13.1, 3.5 Hz, 1H), 1.73 (s, 3H), 1.52 (s, 9H).

tert-Butyl (S)-4-(2,4-Difluoro-5-(((2,2,2-trifluoroethyl)amino)methyl)phenyl)-4-methyl-5,6-dihydro-4H-1,3-thiazin-2-yl)-carbamate (5k). The title compound was prepared from 4 (225 mg, 0.61 mmol) and 2,2,2-trifluoroethan-1-amine (90 mg, 0.91 mmol) according to a similar procedure as for the preparation of 5a in 61% yield. LCMS m/z 454.4 [M – H⁺]. ¹H NMR (400 MHz, CDCl₃) δ 7.28 (t, J = 8.8 Hz, 1H), 6.83 (dd, J = 11.7, 9.4 Hz, 1H), 3.83–3.97 (m, 2H), 3.17 (q, J = 9.2 Hz, 2H), 2.79–2.89 (m, 1H), 2.66–2.79 (m, 1H), 2.57 (dt, J = 12.3, 3.1 Hz, 1H), 2.00–2.11 (m, 1H), 1.70 (s, 3H), 1.50 (s, 9H).

tert-Butyl (S)-4-(5-(((2,2-Difluoroethyl)amino)methyl)-2,4-difluorophenyl)-4-methyl-5,6-dihydro-4H-1,3-thiazin-2-yl)-carbamate (5l). The title compound was prepared from 4 (62 mg, 0.17 mmol) and 2,2-difluoroethan-1-amine (20 mg, 0.25 mmol) according to a similar procedure as for the preparation of 5a in 85% yield. LCMS m/z 436.4 [M – H⁺]. ¹H NMR (400 MHz, CDCl₃) δ 7.24–7.33 (m, 1H), 6.84 (dd, J = 11.7, 9.4 Hz, 1H), 5.67–6.03 (m, 1H), 3.80–3.93 (m, 2H), 2.95 (dt, J = 15.0, 4.3 Hz, 2H), 2.78–2.89 (m, 1H), 2.67–2.78 (m, 1H), 2.51–2.63 (m, 1H), 2.04–2.12 (m, 1H), 1.71 (s, 3H), 1.51 (s, 9H).

tert-Butyl (S)-4-(2,4-Difluoro-5-(((1,1,1-trifluoro-2-methylpropan-2-yl)amino)methyl)phenyl)-4-methyl-5,6-dihydro-4H-1,3-thiazin-2-yl)-carbamate (5m). The title compound was prepared from 4 (52 mg, 0.14 mmol) and 1,1,1-trifluoro-2-methylpropan-2-amine (34 mg, 0.21 mmol) according to a similar procedure as for the preparation of 5a in 58% yield. LCMS m/z 482.3 [M – H⁺]. ¹H NMR (400 MHz, CDCl₃) δ 7.36 (t, J = 8.8 Hz, 1H), 6.81 (dd, J = 11.7, 9.4 Hz, 1H), 3.76–3.99 (m, 2H), 2.70–2.87 (m, 2H), 2.51–2.65 (m, 1H), 1.99–2.13 (m, 1H), 1.63–1.77 (m, 3H), 1.47–1.56 (m, 9H), 1.25–1.34 (m, 6H).

tert-Butyl ((S)-4-(2,4-Difluoro-5-(((R)-1,1,1-trifluoropropan-2-yl)amino)methyl)phenyl)-4-methyl-5,6-dihydro-4H-1,3-thiazin-2-yl)-carbamate (5n). The title compound was prepared from 4 (76 mg, 0.21 mmol) and (R)-1,1,1-trifluoropropan-2-amine (35 mg, 0.31 mmol) according to a similar procedure as for the preparation of 5a in 35% yield. LCMS m/z 468.3 [M – H⁺]. ¹H NMR (400 MHz, CDCl₃) δ 7.29–7.35 (m, 1H), 6.79–6.95 (m, 1H), 3.85–4.00 (m, 2H), 3.12–3.26 (m, 1H), 2.70–2.90 (m, 2H), 2.52–2.70 (m, 1H), 1.98–2.17 (m, 1H), 1.70–1.78 (m, 3H), 1.47–1.57 (m, 9H), 1.27 (d, J = 6.6 Hz, 3H).

tert-Butyl (S)-4-(2,4-Difluoro-5-(((3,3,3-trifluoropropyl)amino)methyl)phenyl)-4-methyl-5,6-dihydro-4H-1,3-thiazin-2-yl)-carbamate (5o). The title compound was prepared from 4 (75 mg, 0.20 mmol) and 3,3,3-trifluoropropan-1-amine (34 mg, 0.30 mmol) according to a similar procedure as for the preparation of 5a in 79% yield. LCMS m/z 468.3 [M – H⁺]. ¹H NMR (400 MHz, CDCl₃) δ 7.23–7.32 (m, 1H), 6.83 (dd, J = 11.5, 9.2 Hz, 1H), 3.72–3.86 (m, 2H), 2.79–2.89 (m, 3H), 2.68–2.79 (m, 1H), 2.57 (dt, J = 12.5, 3.12

Hz, 1H), 2.23–2.41 (m, 2H), 2.00–2.14 (m, 1H), 1.71 (s, 3H), 1.51 (s, 9H).

tert-Butyl (S)-4-(5-(((Cyclopropylamino)methyl)-2,4-difluorophenyl)-4-methyl-5,6-dihydro-4H-1,3-thiazin-2-yl)-carbamate (5p). The title compound was prepared from 4 (54 mg, 0.15 mmol) and cyclopropanamine (12 mg, 0.22 mmol) according to a similar procedure as for the preparation of 5a in 97% yield. LCMS m/z 412.4 [M – H⁺]. ¹H NMR (400 MHz, CDCl₃) δ 7.24 (s, 1H), 6.82 (dd, J = 11.7, 9.4 Hz, 1H), 3.85 (d, J = 7.4 Hz, 2H), 2.80 (d, J = 2.3 Hz, 2H), 2.58 (s, 1H), 1.98–2.14 (m, 2H), 1.65–1.79 (m, 3H), 1.46–1.58 (m, 9H), 0.40–0.50 (m, 2H), 0.31–0.40 (m, 2H).

tert-Butyl (S)-4-(5-(((Cyclopropylmethyl)amino)methyl)-2,4-difluorophenyl)-4-methyl-5,6-dihydro-4H-1,3-thiazin-2-yl)-carbamate (5q). The title compound was prepared from 4 (58 mg, 0.16 mmol) and cyclopropylmethanamine (36 mg, 0.24 mmol) according to a similar procedure as for the preparation of 5a in 57% yield. LCMS m/z 426.4 [M – H⁺]. ¹H NMR (400 MHz, CDCl₃) δ 7.33 (t, J = 8.6 Hz, 1H), 6.81 (dd, J = 11.7, 9.4 Hz, 1H), 3.79–3.93 (m, 2H), 2.78–2.89 (m, 1H), 2.65–2.74 (m, 1H), 2.60 (dt, J = 12.2, 3.2 Hz, 1H), 2.44–2.56 (m, 2H), 2.00–2.11 (m, 1H), 1.98 (s, 1H), 1.68 (s, 3H), 1.50 (s, 9H), 0.93–1.07 (m, 1H), 0.44–0.56 (m, 2H), 0.07–0.20 (m, 2H).

tert-Butyl (S)-4-(5-(((1-(Difluoromethyl)cyclopropyl)amino)methyl)-2,4-difluorophenyl)-4-methyl-5,6-dihydro-4H-1,3-thiazin-2-yl)-carbamate (5r). The title compound was prepared from 4 (55 mg, 0.15 mmol) and 1-(difluoromethyl)cyclopropan-1-amine (32 mg, 0.22 mmol) according to a similar procedure as for the preparation of 5a in 86% yield. LCMS m/z 462.4 [M – H⁺]. ¹H NMR (400 MHz, CDCl₃) δ 7.28 (t, J = 8.8 Hz, 1H), 6.79 (dd, J = 11.7, 9.4 Hz, 1H), 5.41–5.73 (m, 1H), 3.93–4.05 (m, 2H), 2.71–2.84 (m, 2H), 2.52–2.61 (m, 1H), 2.04 (s, 2H), 1.65–1.72 (m, 3H), 1.47–1.54 (m, 9H), 1.13–1.17 (m, 1H), 0.85–0.91 (m, 1H), 0.78–0.84 (m, 3H).

tert-Butyl (S)-4-(5-(((1-Cyanocyclopropyl)amino)methyl)-2,4-difluorophenyl)-4-methyl-5,6-dihydro-4H-1,3-thiazin-2-yl)-carbamate (5s). The title compound was prepared from 4 (45 mg, 0.12 mmol) and 1-aminocyclopropane-1-carbonitrile (17 mg, 0.15 mmol) according to a similar procedure as for the preparation of 5a in 96% yield. LCMS m/z 437.4 [M – H⁺]. ¹H NMR (400 MHz, CDCl₃) δ 7.21 (t, J = 8.8 Hz, 1H), 6.84 (dd, J = 11.7, 9.4 Hz, 1H), 3.96 (q, J = 13.66 Hz, 2H), 2.71–2.84 (m, 2H), 2.54–2.66 (m, 1H), 1.97–2.05 (m, 1H), 1.70 (s, 3H), 1.46–1.57 (m, 9H), 1.18–1.29 (m, 2H), 1.03–1.10 (m, 2H).

(S)-N-(4-(2,4-Difluoro-5-(((3-(trifluoromethyl)oxetan-3-yl)amino)methyl)phenyl)-4-methyl-5,6-dihydro-4H-1,3-thiazin-2-yl)-benzamide (5t). A methanol solution (6.75 mL, 0.1 M) of 4 (250 mg, 0.675 mmol, 1 equiv) was treated with HCl (4 M in dioxane, 3.37 mL, 13.5 mmol, 20 equiv). The resulting yellow solution was stirred at 50 °C for 3 h. The reaction mixture was concentrated under reduced pressure to yield a colorless oil, which was dissolved in H₂O. The resulting solution was extracted with Et₂O (3 \times). The resulting aq layer (pH 1) was basified to pH 10 with 1 N NaOH. The colorless solution was extracted with CH₂Cl₂ (3 \times). The combined organics were washed with brine (1 \times), dried over Na₂SO₄, concentrated, and purified via silica chromatography using a 10% MeOH/1% NH₄OH/89% CH₂Cl₂ mixture as eluent to yield a colorless oil. LCMS m/z 271.3 [M – H⁺]. ¹H NMR (400 MHz, CDCl₃) δ 10.18 (s, 1H), 7.95 (t, J = 8.6 Hz, 1H), 6.81 (dd, J = 11.5, 9.9 Hz, 1H), 4.16–4.56 (m, 2H), 2.89–3.01 (m, 1H), 2.55–2.68 (m, 1H), 2.10–2.21 (m, 1H), 1.85–1.98 (m, 1H), 1.45–1.54 (m, 3H). The purified amidine (135 mg, 0.500 mmol) was immediately dissolved in a 2:1 solution of THF:MeOH (2.1 mL). TEA (0.11 mL, 0.80 mmol) was added followed by benzoic anhydride (150 mg, 0.650 mmol). The reaction was stirred at rt for 18 h. The reaction was then concentrated and redissolved in water and EtOAc. The layers were separated, and the aqueous layer was back extracted with EtOAc (2 \times). The combined organics were washed with water and with brine, dried over sodium sulfate, concentrated, and subjected to silica gel chromatography using a 0–100% EtOAc/heptane gradient. Yield: 86%. LCMS m/z 375.3 [M – H⁺]. The resultant compound (16 mg, 0.09 mmol) was reacted with the HCl salt of 3-(trifluoromethyl)oxetan-3-amine (28 mg, 0.075 mmol), using a similar procedure as for the preparation of 5a in 70% yield. LCMS m/z 500.3 [M – H⁺]. ¹H NMR (400 MHz, CDCl₃) δ 12.23–12.60 (m, 1H), 8.16–8.29 (m,

2H), 7.38–7.56 (m, 4H), 6.82–6.95 (m, 1H), 4.67–4.77 (m, 2H), 4.54 (d, $J = 7.0$ Hz, 2H), 3.89 (d, $J = 7.4$ Hz, 2H), 2.85–2.99 (m, 2H), 2.63–2.74 (m, 1H), 2.10–2.22 (m, 1H), 1.81 (s, 3H), 1.22–1.36 (m, 1H).

tert-Butyl (*S*)-(4-(2,4-Difluoro-5-(((1-(trifluoromethyl)cyclopropyl)amino)methyl)phenyl)-4-methyl-5,6-dihydro-4H-1,3-thiazin-2-yl)carbamate (**5u**). The title compound was prepared from **4** (130 mg, 0.351 mmol) and 1-(trifluoromethyl)cyclopropan-1-amine (66 mg, 0.526 mmol) according to a similar procedure as for the preparation of **5a** in 67% yield. LCMS m/z 480.4 $[M - H]^+$. 1H NMR (400 MHz, $CDCl_3$) δ 7.21–7.28 (m, 1H), 6.72–6.82 (m, 1H), 3.91–4.04 (m, 2H), 2.67–2.84 (m, 2H), 2.47–2.61 (m, 1H), 1.96–2.11 (m, 2H), 1.62–1.74 (m, 3H), 1.44–1.54 (m, 9H), 0.98–1.05 (m, 2H), 0.81–0.90 (m, 2H).

(*S*)-4-(2,4-Difluoro-5-(((5-methylpyridin-2-yl)amino)methyl)phenyl)-4-methyl-5,6-dihydro-4H-1,3-thiazin-2-amine (**6a**). A methanol solution (0.6 mL, 0.1 M) of **5a** (28 mg, 0.06 mmol, 1 equiv) was treated with HCl (4 M in dioxane, 0.3 mL, 4 equiv). The solution was stirred at 50 °C for 2 h. The reaction was then concentrated and redissolved in water. The aqueous solution was extracted with diethyl ether (3 \times) and then brought to pH \sim 12 with 1 N NaOH. This solution was extracted with CH_2Cl_2 (3 \times). The combined organics were dried over sodium sulfate, concentrated, and purified via silica gel chromatography using a 0–60% gradient of a 10% MeOH/1% NH_4OH /89% CH_2Cl_2 solution and CH_2Cl_2 to yield **6a** in 78% yield. LCMS m/z 363.4 $[M - H]^+$. 1H NMR (400 MHz, $CDCl_3$) δ 7.91 (d, $J = 1.6$ Hz, 1H), 7.40 (t, $J = 9.2$ Hz, 1H), 7.24 (dd, $J = 8.2, 2.3$ Hz, 1H), 6.78 (dd, $J = 11.7, 9.4$ Hz, 1H), 6.33 (d, $J = 8.6$ Hz, 1H), 5.10 (t, $J = 5.8$ Hz, 1H), 4.40–4.56 (m, 2H), 2.89 (ddd, $J = 12.2, 6.2, 3.9$ Hz, 1H), 2.59 (dt, $J = 11.5, 3.5$ Hz, 1H), 2.31–2.42 (m, 1H), 2.18 (s, 3H), 1.83 (ddd, $J = 14.0, 10.7, 3.7$ Hz, 1H), 1.57 (d, $J = 1.2$ Hz, 3H).

(*S*)-4-(5-((Ethylamino)methyl)-2,4-difluorophenyl)-4-methyl-5,6-dihydro-4H-1,3-thiazin-2-amine (**6b**). The title compound was prepared from **5b** (142 mg, 0.355 mmol) according to a similar procedure as for the preparation of **6a** in 63% yield. LCMS m/z 300.4 $[M - H]^+$. 1H NMR (400 MHz, $CDCl_3$) δ 7.32 (t, $J = 9.2$ Hz, 1H), 6.76 (dd, $J = 11.7, 9.8$ Hz, 1H), 3.78 (s, 2H), 2.96 (ddd, $J = 12.1, 6.8, 3.7$ Hz, 1H), 2.58–2.74 (m, 3H), 2.33 (ddd, $J = 14.0, 6.7, 3.5$ Hz, 1H), 1.89 (ddd, $J = 13.8, 10.3, 3.9$ Hz, 1H), 1.58 (d, $J = 1.2$ Hz, 3H), 1.11 (t, $J = 7.0$ Hz, 3H).

(*S*)-4-(2,4-Difluoro-5-((isopropylamino)methyl)phenyl)-4-methyl-5,6-dihydro-4H-1,3-thiazin-2-amine (**6c**). Compound **5c** (34 mg, 0.08 mmol, 1 equiv) was dissolved in CH_2Cl_2 (0.41 mL, 0.2 M), and trifluoroacetic acid (126 μ L, 1.64 mmol, 20 equiv) was added. The reaction was stirred at rt for 18 h. The reaction was concentrated and taken up in EtOAc and aqueous saturated sodium bicarbonate. The layers were separated, and the aqueous layer was extracted with EtOAc (2 \times). The combined organics were washed with brine, dried over sodium sulfate, and purified via silica gel chromatography using a 0–60% gradient of a 10% MeOH/1% NH_4OH /89% CH_2Cl_2 solution and CH_2Cl_2 to yield **6c** in 60% yield. LCMS m/z 314.4 $[M - H]^+$. 1H NMR (400 MHz, $CDCl_3$) δ 8.07 (t, $J = 8.5$ Hz, 1H), 6.92 (dd, $J = 9.0, 11.5$ Hz, 1H), 4.78 (s, 2H), 4.15–4.32 (m, 2H), 3.29 (sept, $J = 6.5$ Hz, 1H), 2.96–3.10 (m, 1H), 2.78–2.91 (m, 2H), 2.10–2.24 (m, 1H), 1.82 (s, 3H), 1.49 (dd, $J = 7.5, 6.8$ Hz, 6H).

(*S*)-4-(5-((Dimethylamino)methyl)-2,4-difluorophenyl)-4-methyl-5,6-dihydro-4H-1,3-thiazin-2-amine (**6d**). The title compound was prepared from **5d** (59 mg, 0.15 mmol) according to a similar procedure as for the preparation of **6a** in 90% yield. LCMS m/z 300.3 $[M - H]^+$. 1H NMR (400 MHz, $CDCl_3$) δ 7.32 (t, $J = 9.0$ Hz, 1H), 6.77 (dd, $J = 11.9, 9.6$ Hz, 1H), 4.55 (br s, 1H), 3.47–3.55 (m, 1H), 3.36–3.47 (m, 1H), 2.97 (ddd, $J = 12.1, 6.8, 3.7$ Hz, 1H), 2.68 (ddd, $J = 12.2, 10.2, 3.7$ Hz, 1H), 2.28–2.38 (m, 1H), 2.24 (s, 6H), 1.83–1.96 (m, 1H), 1.59 (d, $J = 1.6$ Hz, 1H).

(*S*)-4-(2,4-Difluoro-5-(((*R*)-3-methoxyprolidin-1-yl)methyl)phenyl)-4-methyl-5,6-dihydro-4H-1,3-thiazin-2-amine (**6e**). The title compound was prepared from **5e** (116 mg, 0.255 mmol) according to a similar procedure as for the preparation of **6a** in 68% yield. LCMS m/z 356.4 $[M - H]^+$. 1H NMR (400 MHz, $CDCl_3$) δ 7.33 (t, $J = 9.0$ Hz, 1H), 6.74 (dd, $J = 11.7, 9.4$ Hz, 1H), 3.86–3.97 (m,

1H), 3.65–3.75 (m, 1H), 3.54–3.63 (m, 1H), 3.25 (s, 3H), 2.93 (ddd, $J = 12.1, 6.4, 3.7$ Hz, 1H), 2.82 (dd, $J = 10.2, 6.2$ Hz, 1H), 2.59–2.69 (m, 2H), 2.47–2.56 (m, 2H), 2.35 (ddd, $J = 14.0, 6.3, 3.5$ Hz, 1H), 1.98–2.10 (m, 1H), 1.71–1.89 (m, 2H), 1.57 (d, $J = 1.6$ Hz, 3H).

(*S*)-4-(2,4-Difluoro-5-(((2-methoxyethyl)amino)methyl)phenyl)-4-methyl-5,6-dihydro-4H-1,3-thiazin-2-amine (**6f**). The title compound was prepared from **6f** (96 mg, 0.22 mmol) according to a similar procedure as for the preparation of **6a** in 56% yield. LCMS m/z 330.4 $[M - H]^+$. 1H NMR (400 MHz, $CDCl_3$) δ 7.34 (t, $J = 9.0$ Hz, 1H), 6.75 (dd, $J = 11.7, 9.8$ Hz, 1H), 3.80 (s, 2H), 3.49 (t, $J = 5.3$ Hz, 2H), 3.33 (s, 3H), 2.95 (ddd, $J = 12.1, 7.0, 3.9$ Hz, 1H), 2.77 (t, $J = 5.1$ Hz, 2H), 2.67 (ddd, $J = 12.1, 10.5, 3.5$ Hz, 1H), 2.32 (ddd, $J = 14.0, 6.7, 3.5$ Hz, 1H), 1.89 (ddd, $J = 14.0, 10.2, 3.5$ Hz, 1H), 1.57 (s, 3H).

(*S*)-4-(2,4-Difluoro-5-(((3-methoxypropyl)amino)methyl)phenyl)-4-methyl-5,6-dihydro-4H-1,3-thiazin-2-amine (**6g**). The title compound was prepared from **6g** (66 mg, 0.15 mmol) according to a similar procedure as for the preparation of **6a** in 68% yield. LCMS m/z 344.4 $[M - H]^+$. 1H NMR (400 MHz, $CDCl_3$) δ 7.33 (t, $J = 9.0$ Hz, 1H), 6.76 (dd, $J = 11.7, 9.8$ Hz, 1H), 3.78 (s, 2H), 3.44 (t, $J = 6.2$ Hz, 2H), 3.32 (s, 3H), 2.96 (ddd, $J = 12.1, 6.6, 3.9$ Hz, 1H), 2.62–2.72 (m, 3H), 2.34 (ddd, $J = 14.0, 6.7, 3.5$ Hz, 1H), 1.88 (ddd, $J = 14.0, 10.4, 3.7$ Hz, 1H), 1.77 (quin, $J = 6.6$ Hz, 2H), 1.58 (d, $J = 1.2$ Hz, 3H).

(*S*)-4-(2,4-Difluoro-5-(((*R*)-1-methoxypropan-2-yl)amino)methyl)phenyl)-4-methyl-5,6-dihydro-4H-1,3-thiazin-2-amine (**6h**). The title compound was prepared from **5h** (97 mg, 0.22 mmol) according to a similar procedure as for the preparation of **6a** in 64% yield. LCMS m/z 344.4 $[M - H]^+$. 1H NMR (400 MHz, $CDCl_3$) δ 7.33 (t, $J = 9.0$ Hz, 1H), 6.76 (dd, $J = 11.7, 9.4$ Hz, 1H), 3.82–3.91 (m, 1H), 3.71–3.80 (m, 1H), 3.29–3.35 (m, 4H), 3.20–3.29 (m, 1H), 2.95 (ddd, $J = 12.2, 6.5, 3.5$ Hz, 1H), 2.81–2.91 (m, 1H), 2.67 (ddd, $J = 12.0, 10.6, 3.9$ Hz, 1H), 2.36 (ddd, $J = 14.0, 6.6, 3.5$ Hz, 1H), 1.87 (ddd, $J = 14.0, 10.4, 3.7$ Hz, 1H), 1.58 (d, $J = 1.2$ Hz, 3H), 1.05 (d, $J = 6.2$ Hz, 3H).

(*S*)-4-(5-((Bicyclo[1.1.1]pentan-1-ylamino)methyl)-2,4-difluorophenyl)-4-methyl-5,6-dihydro-4H-1,3-thiazin-2-amine (**6i**). The title compound was prepared from **5i** (36 mg, 0.08 mmol) according to a similar procedure as for the preparation of **6a** in 49% yield. LCMS m/z 338.4 $[M - H]^+$. 1H NMR (400 MHz, $CDCl_3$) δ 7.34 (t, $J = 9.2$ Hz, 1H), 6.75 (dd, $J = 11.7, 9.8$ Hz, 1H), 3.70–3.84 (m, 2H), 2.96 (td, $J = 12.3, 3.2$ Hz, 1H), 2.62–2.73 (m, 1H), 2.31–2.41 (m, 2H), 1.83–1.94 (m, 1H), 1.76 (s, 6H), 1.57 (d, $J = 1.2$ Hz, 3H).

(*S*)-4-(2,4-Difluoro-5-((methyl(2,2,2-trifluoroethyl)amino)methyl)phenyl)-4-methyl-5,6-dihydro-4H-1,3-thiazin-2-amine (**6j**). The title compound was prepared from **5j** (46 mg, 0.10 mmol) according to a similar procedure as for the preparation of **6a** in 53% yield. LCMS m/z 368.4 $[M - H]^+$. 1H NMR (400 MHz, $CDCl_3$) δ 7.37 (t, $J = 9.0$ Hz, 1H), 6.79 (dd, $J = 11.7, 9.4$ Hz, 1H), 3.67–3.84 (m, 2H), 3.06 (q, $J = 9.6$ Hz, 2H), 2.96 (ddd, $J = 12.1, 6.2, 3.9$ Hz, 1H), 2.66 (dt, $J = 11.4, 3.7$ Hz, 1H), 2.43 (s, 3H), 2.39 (ddd, $J = 10.4, 6.5, 3.3$ Hz, 1H), 1.86 (ddd, $J = 14.0, 10.6, 3.9$ Hz, 1H), 1.61 (d, $J = 1.2$ Hz, 3H).

(*S*)-4-(2,4-Difluoro-5-(((2,2,2-trifluoroethyl)amino)methyl)phenyl)-4-methyl-5,6-dihydro-4H-1,3-thiazin-2-amine (**6k**). The title compound was prepared from **5k** (166 mg, 0.369 mmol) according to a similar procedure as for the preparation of **6a** in 57% yield. LCMS m/z 354.3 $[M - H]^+$. 1H NMR (400 MHz, $CDCl_3$) δ 7.37 (t, $J = 9.0$ Hz, 1H), 6.79 (dd, $J = 11.7, 9.4$ Hz, 1H), 4.42 (br s, 2H), 3.91 (d, $J = 5.8$ Hz, 2H), 3.10–3.23 (m, 2H), 2.98 (ddd, $J = 12.2, 6.7, 3.7$ Hz, 1H), 2.67 (ddd, $J = 12.1, 10.3, 3.7$ Hz, 1H), 2.33 (ddd, $J = 13.8, 6.8, 3.9$ Hz, 1H), 1.91 (ddd, $J = 14.0, 10.2, 3.5$ Hz, 1H), 1.62–1.71 (m, 1H), 1.59 (d, $J = 1.2$ Hz, 3H). ^{13}C NMR (101 MHz, $CDCl_3$) δ 160.9, 158.4, 150.8, 131.2, 130.2, 127.2, 121.7, 104.9, 56.4, 49.8, 46.8, 30.6, 29.6, 23.8. HRMS calcd for $C_{14}H_{17}N_3F_5S$ ($M+1$) 354.1058, found 354.1053.

(*S*)-4-(5-(((2,2-Difluoroethyl)amino)methyl)-2,4-difluorophenyl)-4-methyl-5,6-dihydro-4H-1,3-thiazin-2-amine (**6l**). The title compound was prepared from **5l** (62 mg, 0.14 mmol) according to a similar procedure as for the preparation of **6a** in 46% yield. LCMS m/z 336.4 $[M - H]^+$. 1H NMR (400 MHz, $CDCl_3$) δ 7.36 (t, $J = 9.0$ Hz, 1H), 6.80 (dd, $J = 11.9, 9.6$ Hz, 1H), 5.69–6.05 (m, 1H), 3.78–3.94 (m, 2H), 2.87–3.04 (m, 3H), 2.68 (ddd, $J = 12.2, 10.4, 3.5$ Hz, 1H),

2.35 (ddd, $J = 13.8, 6.6, 3.7$ Hz, 1H), 1.91 (ddd, $J = 14.0, 10.4, 3.7$ Hz, 1H), 1.60 (s, 3H), 1.43–1.58 (m, 1H).

(*S*)-4-(2,4-Difluoro-5-(((1*R*)-1,1-trifluoro-2-methylpropan-2-yl)-amino)methyl)phenyl)-4-methyl-5,6-dihydro-4*H*-1,3-thiazin-2-amine (**6m**). The title compound was prepared from **5m** (39 mg, 0.08 mmol) according to a similar procedure as for the preparation of **6a** in 82% yield. LCMS m/z 382.4 [M – H⁺]. ¹H NMR (400 MHz, CDCl₃) δ 7.41 (t, $J = 9.0$ Hz, 1H), 6.71–6.81 (m, 1H), 3.98–4.43 (m, 2H), 3.78–3.92 (m, 2H), 2.98 (ddd, $J = 12.1, 6.8, 3.7$ Hz, 1H), 2.69 (ddd, $J = 12.3, 10.3, 3.9$ Hz, 1H), 2.35 (ddd, $J = 14.0, 6.8, 3.7$ Hz, 1H), 1.91 (ddd, $J = 14.0, 10.3, 3.7$ Hz, 1H), 1.55–1.63 (m, 3H), 1.47 (t, $J = 7.2$ Hz, 1H), 1.25–1.37 (m, 6H).

(*S*)-4-(2,4-Difluoro-5-(((*R*)-1,1-trifluoropropan-2-yl)amino)methyl)phenyl)-4-methyl-5,6-dihydro-4*H*-1,3-thiazin-2-amine (**6n**). The title compound was prepared from **5n** (34 mg, 0.07 mmol) according to a similar procedure as for the preparation of **6a** in 30% yield. LCMS m/z 368.3 [M – H⁺]. ¹H NMR (400 MHz, CDCl₃) δ 7.32–7.43 (m, 1H), 6.74–6.86 (m, 1H), 3.82–4.01 (m, 1H), 3.12–3.27 (m, 1H), 2.89–3.05 (m, 1H), 2.61–2.75 (m, 1H), 2.30–2.42 (m, 1H), 1.81–1.96 (m, 1H), 1.59–1.63 (m, 5H), 1.25 (d, $J = 6.6$ Hz, 3H).

(*S*)-4-(2,4-Difluoro-5-(((3,3-trifluoropropyl)amino)methyl)phenyl)-4-methyl-5,6-dihydro-4*H*-1,3-thiazin-2-amine (**6o**). The title compound was prepared from **5o** (75 mg, 0.16 mmol) according to a similar procedure as for the preparation of **6a** in 19% yield. LCMS m/z 368.3 [M – H⁺]. ¹H NMR (400 MHz, CDCl₃) δ 7.34 (t, $J = 8.8$ Hz, 1H), 6.78 (dd, $J = 11.7, 9.4$ Hz, 1H), 3.75–3.85 (m, 2H), 2.97 (ddd, $J = 12.1, 6.6, 3.9$ Hz, 1H), 2.85 (t, $J = 7.0$ Hz, 2H), 2.67 (ddd, $J = 12.2, 10.4, 3.5$ Hz, 1H), 2.25–2.39 (m, 3H), 1.89 (ddd, $J = 14.0, 10.4, 3.7$ Hz, 1H), 1.59 (d, $J = 1.6$ Hz, 3H).

(*S*)-4-(5-((Cyclopropylamino)methyl)-2,4-difluorophenyl)-4-methyl-5,6-dihydro-4*H*-1,3-thiazin-2-amine (**6p**). The title compound was prepared from **5p** (58 mg, 0.14 mmol) according to a similar procedure as for the preparation of **6a** in 19% yield. LCMS m/z 312.3 [M – H⁺]. ¹H NMR (400 MHz, CDCl₃) δ 7.32 (t, $J = 9.0$ Hz, 1H), 6.77 (dd, $J = 11.9, 9.6$ Hz, 1H), 3.79–3.89 (m, 2H), 2.96 (ddd, $J = 12.1, 6.4, 3.7$ Hz, 1H), 2.67 (ddd, $J = 12.2, 10.6, 3.7$ Hz, 1H), 2.37 (ddd, $J = 14.0, 6.4, 3.7$ Hz, 1H), 2.06–2.12 (m, 1H), 1.88 (ddd, $J = 14.0, 10.4, 3.7$ Hz, 1H), 1.59 (d, $J = 1.2$ Hz, 3H), 0.40–0.47 (m, 2H), 0.34–0.40 (m, 2H).

(*S*)-4-(5-(((Cyclopropylmethyl)amino)methyl)-2,4-difluorophenyl)-4-methyl-5,6-dihydro-4*H*-1,3-thiazin-2-amine (**6q**). The title compound was prepared from **5q** (38 mg, 0.09 mmol) according to a similar procedure as for the preparation of **6a** in 34% yield. LCMS m/z 327.4 [M – H⁺]. ¹H NMR (400 MHz, CDCl₃) δ 7.32 (t, $J = 9.2$ Hz, 1H), 6.75 (dd, $J = 11.9, 9.6$ Hz, 1H), 3.80 (s, 2H), 2.96 (ddd, $J = 12.2, 6.7, 3.7$ Hz, 1H), 2.67 (ddd, $J = 12.3, 10.3, 3.9$ Hz, 1H), 2.39–2.52 (m, 2H), 2.34 (ddd, $J = 14.0, 6.7, 3.9$ Hz, 1H), 1.89 (ddd, $J = 14.0, 10.4, 3.7$ Hz, 1H), 1.58 (d, $J = 1.6$ Hz, 3H), 0.88–1.03 (m, 1H), 0.41–0.50 (m, 2H), 0.04 to 0.13 (m, 2H).

(*S*)-4-(5-(((1-(Difluoromethyl)cyclopropyl)amino)methyl)-2,4-difluorophenyl)-4-methyl-5,6-dihydro-4*H*-1,3-thiazin-2-amine (**6r**). The title compound was prepared from **5r** (39 mg, 0.08 mmol) according to a similar procedure as for the preparation of **6a** in 58% yield. LCMS m/z 362.4 [M – H⁺]. ¹H NMR (400 MHz, CDCl₃) δ 7.35 (t, $J = 9.0$ Hz, 1H), 6.69–6.80 (m, 1H), 5.45–5.79 (m, 1H), 4.29 (br s, 2H), 3.98 (d, $J = 7.0$ Hz, 2H), 2.96 (ddd, $J = 12.1, 6.6, 3.9$ Hz, 1H), 2.67 (ddd, $J = 12.1, 10.5, 3.5$ Hz, 1H), 2.35 (ddd, $J = 14.0, 6.6, 3.5$ Hz, 1H), 2.05 (t, $J = 6.8$ Hz, 1H), 1.88 (ddd, $J = 14.0, 10.4, 3.7$ Hz, 1H), 1.52–1.62 (m, 3H), 0.78–0.86 (m, 4H).

(*S*)-1-(5-(2-Amino-4-methyl-5,6-dihydro-4*H*-1,3-thiazin-4-yl)-2,4-difluorobenzyl)amino)cyclopropane-1-carbonitrile (**6s**). The title compound was prepared from **5s** (51 mg, 0.12 mmol) according to a similar procedure as for the preparation of **6a** in 48% yield. LCMS m/z 337.4 [M – H⁺]. ¹H NMR (400 MHz, CDCl₃) δ 7.34 (t, $J = 9.0$ Hz, 1H), 6.78 (dd, $J = 11.7, 9.4$ Hz, 1H), 3.90–4.02 (m, 2H), 2.95 (ddd, $J = 12.2, 6.5, 3.9$ Hz, 1H), 2.69 (ddd, $J = 12.1, 10.5, 3.5$ Hz, 1H), 2.36 (ddd, $J = 14.0, 6.6, 3.5$ Hz, 1H), 1.88 (ddd, $J = 14.0, 10.5, 3.5$ Hz, 1H), 1.54–1.61 (m, 3H), 1.16–1.25 (m, 2H), 1.00–1.09 (m, 2H).

(*S*)-4-(2,4-Difluoro-5-(((3-(trifluoromethyl)oxetan-3-yl)amino)methyl)phenyl)-4-methyl-5,6-dihydro-4*H*-1,3-thiazin-2-amine (**6t**).

To an ethanolic solution of **5t** (26 mg, 0.052 mmol) was added hydrazine monohydrate (27.6 μ L, 0.364 mmol). The resulting solution was allowed to stir at rt for 4 h, at which point the reaction was concentrated under reduced pressure. The residue was subjected to silica chromatography using a 10% MeOH/1% NH₄OH/89% CH₂Cl₂ mixture as eluent to yield **6t** as a colorless oil. Yield: 31%. LCMS m/z 396.4 [M – H⁺]. ¹H NMR (400 MHz, CDCl₃) δ 7.45 (t, $J = 9.0$ Hz, 1H), 6.80 (dd, $J = 11.7, 9.8$ Hz, 1H), 4.77 (dd, $J = 7.0, 1.6$ Hz, 2H), 4.61 (d, $J = 6.2$ Hz, 2H), 3.88 (d, $J = 7.4$ Hz, 2H), 2.94–3.04 (m, 1H), 2.64–2.75 (m, 1H), 2.33 (ddd, $J = 13.8, 6.8, 3.5$ Hz, 1H), 1.82–1.99 (m, 2H), 1.59 (d, $J = 1.2$ Hz, 3H).

(*S*)-4-(2,4-Difluoro-5-(((1-(trifluoromethyl)cyclopropyl)amino)methyl)phenyl)-4-methyl-5,6-dihydro-4*H*-1,3-thiazin-2-amine (**6u**). The title compound was prepared from **5u** (114 mg, 0.238 mmol) according to a similar procedure as for the preparation of **6a** in 63% yield. LCMS m/z 380.4 [M – H⁺]. ¹H NMR (400 MHz, CDCl₃) δ 7.32 (t, $J = 9.0$ Hz, 1H), 6.70–6.79 (m, 1H), 3.92–4.03 (m, 2H), 2.90–2.99 (m, 1H), 2.60–2.71 (m, 1H), 2.30–2.41 (m, 1H), 1.97–2.10 (m, 1H), 1.83–1.93 (m, 1H), 1.58 (s, 3H), 0.99–1.06 (m, 2H), 0.85–0.94 (m, 2H). ¹³C NMR (100 MHz, CDCl₃) δ 160.8, 158.4, 150.8, 130.6, 129.4, 128.4, 125.6, 122.8, 104.5, 56.1, 44.6, 39.9, 30.4, 29.4, 23.6, 11.7. HRMS calcd for C₁₆H₁₈N₃F₃SNa (M + Na) 402.1017, found 402.1034.

tert-Butyl ((4*S*,6*R*)-4-(2,4-Difluoro-5-formylphenyl)-4,6-dimethyl-5,6-dihydro-4*H*-1,3-thiazin-2-yl)carbamate (**10**). To a cooled solution (–78 °C) of **9**²⁰ (230 mg, 0.53 mmol) in anhydrous ether (5.3 mL) was added methylolithium (0.4 mL, 0.61 mmol) dropwise. The mixture was stirred for 30 min before *n*-BuLi (0.27 mL, 0.74 mmol) was added dropwise at –78 °C. The reaction mixture was stirred for another 30 min before the addition of DMF (0.41 mL, 5.3 mmol) in one portion. The reaction was stirred for 1 h and slowly warmed up to –20 °C, then quenched with aq NH₄Cl (10 mL). The layers were separated, and the aqueous layer was extracted with EtOAc (2 \times). The combined organic layers were washed with brine (1 \times), dried (Na₂SO₄), concentrated, and purified by silica chromatography using a 0–40% EtOAc/heptane gradient to yield the product as a colorless solid. Yield: 89%. LCMS m/z 385.3 [M – H⁺]. ¹H NMR (400 MHz, CDCl₃) δ 10.22 (s, 1H), 7.74 (t, $J = 8.4$ Hz, 1H), 6.93 (dd, $J = 11.7, 9.8$ Hz, 1H), 2.65–2.86 (m, 2H), 1.70–1.75 (m, 1H), 1.68 (s, 3H), 1.51 (s, 9H), 1.24 (d, $J = 6.6$ Hz, 3H).

tert-Butyl ((4*S*,6*R*)-4-(2,4-Difluoro-5-(((1-(trifluoromethyl)cyclopropyl)amino)methyl)phenyl)-4,6-dimethyl-5,6-dihydro-4*H*-1,3-thiazin-2-yl)carbamate (**11**). The title compound was prepared from **10** (30 mg, 0.08 mmol) and 1-(trifluoromethyl)cyclopropan-1-amine (39 mg, 0.31 mmol) according to a similar procedure as for the preparation of **5a** in 93% yield. LCMS m/z 494.4 [M – H⁺]. ¹H NMR (400 MHz, CDCl₃) δ 7.21 (t, $J = 8.6$ Hz, 1H), 6.75–6.85 (m, 1H), 4.00 (br s, 2H), 2.81 (d, $J = 13.3$ Hz, 2H), 2.02–2.15 (m, 1H), 1.71 (s, 3H), 1.54 (s, 9H), 1.23–1.33 (m, 3H), 1.00–1.11 (m, 2H), 0.86–0.97 (m, 2H).

(4*S*,6*R*)-4-(2,4-Difluoro-5-(((1-(trifluoromethyl)cyclopropyl)amino)methyl)phenyl)-4,6-dimethyl-5,6-dihydro-4*H*-1,3-thiazin-2-amine (**12**). The title compound was prepared from **11** (35 mg, 0.07 mmol) according to a similar procedure as for the preparation of **6a** in 19% yield. LCMS m/z 394.3 [M – H⁺]. ¹H NMR (400 MHz, CDCl₃) δ 7.07 (t, $J = 9.0$ Hz, 1H), 6.67 (dd, $J = 11.7, 9.4$ Hz, 1H), 3.79–3.98 (m, 2H), 2.66–2.73 (m, 1H), 2.56–2.65 (m, 1H), 1.91–2.03 (m, 1H), 1.55 (s, 3H), 1.15 (d, $J = 6.6$ Hz, 3H), 0.92–0.98 (m, 2H), 0.77–0.86 (m, 2H).

N-((4*aR*,6*R*,8*aS*)-8*a*-(5-Cyano-2,4-difluorophenyl)-6-(fluoromethyl)-4,4*a*,5,6,8*a*-hexahydro-2*H*-pyran[3,4-*d*][1,3]thiazin-2-yl)benzamide (**14**). An oven-dried pressure tube, equipped with a stir bar, was charged with **13**²⁶ (19.0 g, 38.0 mmol), Pd₂(dba)₃ (0.438 g, 0.761 mmol), dppf (0.888 g, 1.52 mmol), zinc (0.302 g, 4.57 mmol), and Zn(CN)₂ (3.35 g, 28.5 mmol). After the flask had been purged with N₂, DMA (70 mL, anhydrous) was added to yield a black solution, which was heated to 130 °C for 16 h. The reaction mixture was cooled and partitioned between EtOAc and NaHCO₃ (aq satd). The organic layer was isolated and the aq was back-extracted with EtOAc (3 \times). The combined organics were washed with H₂O (2 \times) and with brine (1 \times), dried over Na₂SO₄, filtered, and concentrated

under reduced pressure. Flash column chromatography of the organic crude, using a gradient of EtOAc in heptanes (0–100%) afforded **13** (14.5 g, 32.5 mmol, 85% yield) as a white solid.

N-((4*aR*,6*R*,8*aS*)-8*a*-(5-(Aminomethyl)-2,4-difluorophenyl)-6-(fluoromethyl)-4,4*a*,5,6,8,8*a*-hexahydropyrano[3,4-*d*][1,3]thiazin-2-yl)benzamide (**15**). To a metal pressure vessel equipped with a stir bar was added H₂O (40 mL) followed by RaNi (24 g, wet). The H₂O layer was decanted (with a bare minimum left behind to keep the RaNi wet). This process was repeated 3× with H₂O, followed by 3× with EtOH. To the final EtOH solution of RaNi was added EtOH (140 mL). A solution of **13** (14.48 g, 32.5 mmol) in THF (140 mL, anhydrous) and TEA (20 mL, 196 mmol) was added to the vessel, followed by addition of Boc anhydride (22 g, 196 mmol). The reaction vessel was closed and purged with N₂ (3×) followed by H₂ (3×). Once the purging was completed, the reaction vessel was placed under a H₂ atmosphere of 70 PSI and was left stirring at rt until complete consumption of starting material was observed. The reaction mixture was filtered through a Celite pad, which was then washed 3× with MeOH. The filtrates were concentrated under reduced pressure and redissolved in MeOH (300 mL). The resulting solution was treated with HCl (4 M in dioxane, 162.6 mL, 650 mmol). Once the Boc-deprotection was complete, the reaction mixture was concentrated under reduced pressure, redissolved in CH₂Cl₂, and treated with NaOH (1 N, 1 L, aq). The resulting biphasic solution was left stirring at rt for 15 min. After that time, the layers were separated and the aq layer was washed with CH₂Cl₂ (3 × 200 mL). The combined organic layers were dried over Na₂SO₄, filtered, and concentrated under reduced pressure. Flash column chromatography of the organic crude, using a gradient of MeOH in CH₂Cl₂ (0–5%), afforded **14** (9.0 g, 20 mmol, 61% yield) as a white solid.

(4*aR*,6*R*,8*aS*)-8*a*-(2,4-Difluoro-5-(((2,2,2-trifluoroethyl)amino)methyl)phenyl)-6-(fluoromethyl)-4,4*a*,5,6,8,8*a*-hexahydropyrano[3,4-*d*][1,3]thiazin-2-amine (**16**). In a pressure tube equipped with a stir bar, under N₂, an acetonitrile (225 mL, anhydrous) solution of **15** (4.76 g, 10.6 mmol) was treated with TEA (2.21 mL, 15.9 mmol) and 2,2,2-trifluoroethyl trifluoromethanesulfonate (2.29 mL, 15.9 mmol). The resulting solution was stirred at 70 °C until the starting material had been completely consumed. The reaction mixture was cooled down to rt and concentrated under reduced pressure. The organic crude was partitioned between H₂O (150 mL) and EtOAc (150 mL). The layers were separated, and the aq layer was back-extracted with EtOAc (2×). The combined organics were then washed with brine (1×), dried over Na₂SO₄, filtered, and concentrated under reduced pressure to afford *N*-((4*aR*,6*R*,8*aS*)-8*a*-(2,4-difluoro-5-(((2,2,2-trifluoroethyl)amino)methyl)phenyl)-6-(fluoromethyl)-4,4*a*,5,6,8,8*a*-hexahydropyrano[3,4-*d*][1,3]thiazin-2-yl)benzamide (4.72 g, 8.88 mmol, 84% yield) as a yellow solid.

DBU (0.947 mL, 6.01 mmol) was added to a methanol solution (407 mL, anhydrous) of *N*-((4*aR*,6*R*,8*aS*)-8*a*-(2,4-difluoro-5-(((2,2,2-trifluoroethyl)amino)methyl)phenyl)-6-(fluoromethyl)-4,4*a*,5,6,8,8*a*-hexahydropyrano[3,4-*d*][1,3]thiazin-2-yl)benzamide (4.58 g, 8.62 mmol). The resulting solution was heated to 70 °C until complete consumption of starting material was observed. The reaction mixture was concentrated under reduced pressure. Flash column chromatography of the organic crude, using a gradient of MeOH in CH₂Cl₂ (0–20%), afforded **16** (2.60 g, 6.08 mmol, 71% yield) as a white foam. ¹H NMR (400 MHz, CDCl₃) δ 1.43–1.51 (m, 1H) 1.87 (qd, *J* = 12.3, 2.5 Hz, 1H) 2.62 (dd, *J* = 12.1, 2.3 Hz, 1H) 2.87–3.00 (m, 2H) 3.08–3.21 (m, 2H) 3.82 (d, *J* = 11.3 Hz, 1H) 3.86–3.99 (m, 3H) 4.10 (dd, *J* = 11.1, 2.2 Hz, 1H) 4.34–4.46 (m, 1H) 4.46–4.58 (m, 1H) 4.94 (br s, 1H) 6.81 (dd, *J* = 11.7, 9.4 Hz, 1H) 7.34 (t, *J* = 8.8 Hz, 1H). ¹³C NMR (400 MHz, CDCl₃) δ 26.55, 28.46, 28.97, 46.29, 58.31, 75.37, 84.36, 86.06, 104.92, 122.18, 124.95, 132.54, 157.17, 159.08, 159.69, 161.56.

■ ASSOCIATED CONTENT

Supporting Information

The Supporting Information is available free of charge on the ACS Publications website at DOI: 10.1021/acs.jmedchem.6b01451.

Data collection and refinement statistics for crystal structures of BACE1 with **6u** and **16**, and CYP 2D6 with **6u** and **12** (PDF)

Molecular formula strings (CSV)

■ Accession Codes

Atomic coordinates and structure factors for the following BACE1 cocrystal structures have been deposited with the RCSB: compound **6u** (PDB: 5T1U), compound **16** (PDB: 5T1W). Atomic coordinates and structure factors have been deposited with the RCSB for crystal structures of CYP 2D6 complexed with compound **6u** (PDB: 5TFT), and with compound **12** (PDB:5TFU).

■ AUTHOR INFORMATION

Corresponding Author

*Phone: 617 395 0670. E-mail: christopher.r.butler@pfizer.com.

ORCID

Christopher R. Butler: 0000-0002-9387-5011

Notes

The authors declare no competing financial interest.

■ ACKNOWLEDGMENTS

We thank David Karanian for toxicology expertise, Leslie Pustilnik, Stephen Noell, Carol Menard, and Theresa Dickinson for the generation of in vitro data and assay reagents, as well as Romelia Salomon-Ferrer, Katherine Brighty, and Pat Verhoest for helpful discussion in manuscript preparation. Use of the IMCA-CAT beamline 17-ID at the Advanced Photon Source was supported by the companies of the Industrial Macromolecular Crystallography Association through a contract with Hauptman-Woodward Medical Research Institute. Use of the Advanced Photon Source was supported by the U.S. Department of Energy, Office of Science, Office of Basic Energy Sciences, under contract no. DE-AC02-06CH11357. This work was supported in part by NIH grant GM031001. The content of this manuscript is solely the responsibility of the authors and does not necessarily represent the official views of the National Institutes of Health. Data collection for crystals of the P450 CYP 2D6 complexes was carried out at the Stanford Synchrotron Radiation Lightsource, a national user facility operated by Stanford University on behalf of the United States Department of Energy, Office of Basic Energy Sciences under Contact No. DE-AC02-762F00515. The Stanford Synchrotron Radiation Lightsource Structural Molecular Biology Program is supported by the United States Department of Energy, Office of Biological and Environmental Research and by the National Center for Research Resources, Biomedical Technology Program, and NIGMS (including P41GM103393) of the National Institutes of Health.

■ ABBREVIATIONS USED

BACE1, β -secretase; sAPP β , N-terminal ectodomain of APP; C99, C-terminal fragment; hERG, human ether-a-go-go-related gene; CatD, cathepsin D; RPE, retinal pigment epithelium; P-gp, P-glycoprotein; $C_{b,u}/C_{p,u}$ ratio of unbound concentration in brain to the unbound concentration in plasma; CFA, cell-free assay; WCA, whole-cell assay; HLM, human liver microsomes; LipE, lipophilic efficiency; EWG, electron-withdrawing group; Er, efflux ratio; C_{eff} , efficacious concentration; DELFIA, dissociation-enhanced lanthanide fluorescent immunoassay

REFERENCES

- (1) Hardy, J.; Allsop, D. Amyloid deposition as the central event in the aetiology of Alzheimer's disease. *Trends Pharmacol. Sci.* **1991**, *12*, 383–388.
- (2) Tanzi, R. E.; Bertram, L. Twenty years of the Alzheimer's disease amyloid hypothesis: A genetic perspective. *Cell* **2005**, *120*, 545–555.
- (3) De Strooper, B. Proteases and proteolysis in Alzheimer Disease: a multifactorial view on the disease process. *Physiol. Rev.* **2010**, *90*, 465–494.
- (4) Vassar, R.; Kovacs, D. M.; Yan, R.; Wong, P. C. The beta-secretase enzyme BACE in health and Alzheimer's disease: regulation, cell biology, function, and therapeutic potential. *J. Neurosci.* **2009**, *29*, 12787–12794.
- (5) Marks, N.; Berg, M. J. BACE and gamma-secretase characterization and their sorting as therapeutic targets to reduce amyloidogenesis. *Neurochem. Res.* **2010**, *35*, 181–210.
- (6) Jonsson, T.; Atwal, J. K.; Steinberg, S.; Snaedal, J.; Jonsson, P. V.; Bjornsson, S.; Stefansson, H.; Sulem, P.; Gudbjartsson, D.; Maloney, J.; Hoyte, K.; Gustafson, A.; Liu, Y.; Lu, Y.; Bhargale, T.; Graham, R. R.; Huttenlocher, J.; Bjornsdottir, G.; Andreassen, O. A.; Jonsson, E. G.; Palotie, A.; Behrens, T. W.; Magnusson, O. T.; Kong, A.; Thorsteinsdottir, U.; Watts, R. J.; Stefansson, K. A mutation in APP protects against Alzheimer's disease and age-related cognitive decline. *Nature* **2012**, *488*, 96–99.
- (7) Evin, G.; Hince, C. BACE1 as a therapeutic target in Alzheimer's disease: rationale and current status. *Drugs Aging* **2013**, *30*, 755–764.
- (8) (a) Sanguinetti, M. C.; Tristani-Firouzi, M. hERG potassium channels and cardiac arrhythmia. *Nature* **2006**, *440*, 463–469. (b) Sanguinetti, M. C.; Jiang, C.; Curran, M. E.; Keating, M. T. A mechanistic link between an inherited and an acquired cardiac arrhythmia: hERG encodes the IKr potassium channel. *Cell* **1995**, *81*, 299–307. (c) Roden, D. M. Drug-induced prolongation of the QT interval. *N. Engl. J. Med.* **2004**, *350*, 1013–1022.
- (9) May, P. C.; Dean, R. A.; Lowe, S. L.; Martenyi, F.; Sheehan, S. M.; Boggs, L. N.; Monk, S. A.; Mathes, B. M.; Mergott, D. J.; Watson, B. M.; Stout, S. L.; Timm, D. E.; Smith LaBell, E.; Gonzales, C. R.; Nakano, M.; Jhee, S. S.; Yen, M.; Ereshefsky, L.; Lindstrom, T. D.; Calligaro, D. O.; Cocke, P. J.; Hall, D. G.; Friedrich, S.; Citron, M.; Audia, J. E. Robust central reduction of amyloid- β in humans with an orally available, non-peptidic β -secretase inhibitor. *J. Neurosci.* **2011**, *31*, 16507–16516.
- (10) (a) Waring, M. J.; Johnstone, C. A quantitative assessment of hERG liability as a function of lipophilicity. *Bioorg. Med. Chem. Lett.* **2007**, *17*, 1759–1764. (b) Jamieson, C.; Moir, E. M.; Rankovic, Z.; Wishart, G. Medicinal chemistry of hERG optimizations: highlights and hang-ups. *J. Med. Chem.* **2006**, *49*, 5029–5046.
- (11) Rochin, L.; Hurbain, L.; Serneels, L.; Fort, C.; Watt, B.; Leblanc, P.; Marks, M. S.; De Strooper, B.; Raposo, G.; van Niel, G. BACE2 processes PMEL to form the melanosome amyloid matrix in pigment cells. *Proc. Natl. Acad. Sci. U. S. A.* **2013**, *110*, 10658–10663.
- (12) Shimshek, D. R.; Jacobson, L. H.; Kolly, C.; Zamurovic, N.; Balavenkatraman, K. K.; Morawiec, L.; Kreutzer, R.; Schelle, J.; Jucker, M.; Bertschi, B.; Theil, D.; Heier, A.; Bigot, K.; Beltz, K.; Machauer, R.; Brzak, I.; Perrot, L.; Neumann, U. Pharmacological BACE1 and BACE2 inhibition induces hair depigmentation by inhibiting PMEL17 processing in mice. *Sci. Rep.* **2016**, *6*, 21917.
- (13) Oehlrich, D.; Prokopcova, H.; Gijssen, H. J. The evolution of amidine-based brain penetrant BACE1 inhibitors. *Bioorg. Med. Chem. Lett.* **2014**, *24*, 2033–2045.
- (14) (a) Woltering, T. J.; Wostl, W.; Hilpert, H.; Rogers-Evans, M.; Pinard, E.; Mayweg, A.; Gobel, M.; Banner, D. W.; Benz, J.; Travagli, M.; Pollastrini, M.; Marconi, G.; Gabellieri, E.; Guba, W.; Mauser, H.; Andreini, M.; Jacobsen, H.; Power, E.; Narquizian, R. BACE1 inhibitors: a head group scan on a series of amides. *Bioorg. Med. Chem. Lett.* **2013**, *23*, 4239–4243. (b) Hilpert, H.; Guba, W.; Woltering, T. J.; Wostl, W.; Pinard, E.; Mauser, H.; Mayweg, A. V.; Rogers-Evans, M.; Humm, R.; Krummenacher, D.; Muser, T.; Schneider, C.; Jacobsen, H.; Ozmen, L.; Bergadano, A.; Banner, D. W.; Hochstrasser, R.; Kuglstatler, A.; David-Pierson, P.; Fischer, H.; Polara, A.; Narquizian, R. beta-Secretase (BACE1) inhibitors with high in vivo efficacy suitable for clinical evaluation in Alzheimer's disease. *J. Med. Chem.* **2013**, *56*, 3980–3995. (c) Rombouts, F. J. R.; Tresadern, G.; Delgado, O.; Martínez-Lamenca, C.; Van Gool, M.; García-Molina, A.; Alonso de Diego, S. A.; Oehlrich, D.; Prokopcova, H.; Alonso, J. M.; Austin, N.; Borghys, H.; Van Brandt, S.; Surkyn, M.; De Cley, M.; Vos, A.; Alexander, R.; Macdonald, G.; Moechars, D.; Gijssen, H.; Trabanco, A. A. 1,4-Oxazine β -secretase 1 (BACE1) inhibitors: from hit generation to orally bioavailable brain penetrant leads. *J. Med. Chem.* **2015**, *58*, 8216–8235.
- (15) Wager, T. T.; Hou, X.; Verhoest, P. R.; Villalobos, A. Moving beyond rules: the development of a central nervous system multiparameter optimization (CNS MPO) approach to enable alignment of druglike properties. *ACS Chem. Neurosci.* **2010**, *1*, 435–449.
- (16) (a) Dislich, B.; Lichtenthaler, S. F. The membrane-bound aspartyl protease BACE1: molecular and functional properties in Alzheimer's disease and beyond. *Front. Physiol.* **2012**, *3*, 8. (b) Decourt, B. S.; Marwan, N. BACE1 as a potential biomarker for Alzheimer's Disease. *J. Alzheimers Dis.* **2011**, *24* (Suppl 2), 53–59. (c) Cole, S. L.; Vassar, R. The Alzheimer's disease β -secretase enzyme, BACE1. *Mol. Neurodegener.* **2007**, *2*, 22. (d) Georgievskaa, B.; Gustavsson, S.; Lundkvist, J.; Neelissen, J.; Eketjäll, S.; Ramberg, V.; Bueters, T.; Agerman, K.; Juréus, A.; Svensson, S.; Berg, S.; Fälting, J.; Lendahl, U. Revisiting the peripheral sink hypothesis: inhibiting BACE1 activity in the periphery does not alter β -amyloid levels in the CNS. *J. Neurochem.* **2015**, *132*, 477–486.
- (17) Wu, Y.-J.; Guernon, J.; Yang, F.; Snyder, L.; Shi, J.; McClure, A.; Rajamani, R.; Park, H.; Ng, A.; Lewis, H.; Chang, C. Y.; Camac, D.; Toyn, J. H.; Ahlijanian, M. K.; Albright, C. F.; Macor, J. E.; Thompson, L. A. Targeting the BACE1 active site flap leads to a potent inhibitor that elicits robust brain A β reduction in rodents. *ACS Med. Chem. Lett.* **2016**, *7*, 271–276.
- (18) Stepan, A. F.; Walker, D. P.; Bauman, J.; Price, D. A.; Baillie, T. A.; Kalgutkar, A. S.; Aleo, M. D. Structural alert/reactive metabolite concept as applied in medicinal chemistry to mitigate the risk of idiosyncratic drug toxicity: a perspective based on the critical examination of trends in the top 200 drugs marketed in the United States. *Chem. Res. Toxicol.* **2011**, *24*, 1345–1410.
- (19) Hilpert, H.; Guba, W.; Woltering, T. J.; Wostl, W.; Pinard, E.; Mauser, H.; Mayweg, A. V.; Rogers-Evans, M.; Humm, R.; Krummenacher, D.; Muser, T.; Schneider, C.; Jacobsen, H.; Ozmen, L.; Bergadano, A.; Banner, D. W.; Hochstrasser, R.; Kuglstatler, A.; David-Pierson, P.; Fischer, H.; Polara, A.; Narquizian, R. β -Secretase (BACE1) inhibitors with high in vivo efficacy suitable for clinical evaluation in Alzheimer's disease. *J. Med. Chem.* **2013**, *56*, 3980–3995.
- (20) Audia, J. E.; Mergot, D. J.; Sheehan, S. M.; Watson, B. M. Aminodihydrothiazine derivatives as BACE inhibitors for the treatment of Alzheimer's disease. WO2009134617, 2009.
- (21) Butler, C. R.; Brodney, M. A.; Beck, E. M.; Barreiro, G.; Nolan, C. E.; Pan, F.; Vajdos, F.; Parris, K.; Varghese, A. H.; Helal, C. J.; Lira, R.; Doran, S. D.; Riddell, D. R.; Buzon, L. M.; Dutra, J. K.; Martinez-Alsina, L. A.; Ogilvie, K.; Murray, J. C.; Young, J. M.; Atchison, K.; Robshaw, A.; Gonzales, C.; Wang, J.; Zhang, Y.; O'Neill, B. T. Discovery of a series of efficient, centrally efficacious BACE1 inhibitors through structure-based drug design. *J. Med. Chem.* **2015**, *58*, 2678–2702.
- (22) Shalaeva, M.; Kenseth, J.; Lombardo, F.; Bastin, A. Measurement of dissociation constants (pK_a values) of organic compounds by multiplexed capillary electrophoresis using aqueous and cosolvent buffers. *J. Pharm. Sci.* **2008**, *97*, 2581–2606.
- (23) Lu, Y.; Riddell, D.; Hajos-Korcsok, E.; Bales, K.; Wood, K. M.; Nolan, C. E.; Robshaw, A. E.; Zhang, L.; Leung, L.; Becker, S. L.; Tseng, E.; Barricklow, J.; Miller, E. H.; Osgood, S.; O'Neill, B. T.; Brodney, M. A.; Johnson, D. S.; Pettersson, M. Cerebrospinal fluid amyloid- β (A β) as an effect biomarker for brain A β lowering verified by quantitative preclinical analyses. *J. Pharmacol. Exp. Ther.* **2012**, *342*, 366–375.

(24) (a) Rendic, S.; Carlo, F. J. D. Human cytochrome P450 enzymes: a status report summarizing their reactions, substrates, inducers, and inhibitors. *Drug Metab. Rev.* **1997**, *29*, 413–580.

(b) Teh, L. K.; Bertilsson, L. Pharmacogenomics of CYP 2D6: molecular genetics, interethnic differences and clinical importance. *Drug Metab. Pharmacokinet.* **2012**, *27*, 55–67. (c) Bertilsson, L.; Dahl, M.-L.; Dalén, P.; Al-Shurbaji, A. Molecular genetics of CYP 2D6: Clinical relevance with focus on psychotropic drugs. *br J. Clin. Pharmacol.* **2002**, *53*, 111–122.

(25) Brodney, M. A.; Beck, E. M.; Butler, C. R.; Barreiro, G.; Johnson, E. F.; Riddell, D.; Parris, K.; Nolan, C. E.; Fan, Y.; Atchison, K.; Gonzales, C.; Robshaw, A. E.; Doran, S. D.; Bundesmann, M. W.; Buzon, L.; Dutra, J.; Henegar, K.; LaChapelle, E.; Hou, X.; Rogers, B. N.; Pandit, J.; Lira, R.; Martinez-Alsina, L.; Mikochik, P.; Murray, J. C.; Ogilvie, K.; Price, L.; Sakya, S. M.; Yu, A.; Zhang, Y.; O'Neill, B. T. Utilizing structures of CYP 2D6 and BACE1 complexes to reduce risk of drug–drug interactions with a novel series of centrally efficacious BACE1 inhibitors. *J. Med. Chem.* **2015**, *58*, 3223–3252.

(26) Compound **13** was prepared in analogous fashion to ref **21**. Preparation and characterization information is included in the [Supporting Information](#).

(27) Kalvass, J. C.; Maurer, T. S. Influence of nonspecific brain and plasma binding on CNS exposure: implications for rational drug discovery. *Biopharm. Drug Dispos.* **2002**, *23*, 327–338.

(28) Kutchinsky, J.; Friis, S.; Asmild, M.; Taborski, R.; Pedersen, S.; Vestergaard, R. K.; Jacobsen, R. B.; Krzywkowski, K.; Schroder, R. L.; Ljungstrom, T.; Helix, N.; Sorensen, C. B.; Bech, M.; Willumsen, N. J. Characterization of potassium channel modulators with QPatch automated patch-clamp technology: system characteristics and performance. *Assay Drug Dev. Technol.* **2003**, *1*, 685–693.

(29) Bridges, K. G.; Chopra, R.; Lin, L.; Svenson, K.; Tam, A.; Jin, G.; Cowling, R.; Lovering, F.; Akopian, T. N.; DiBlasio-Smith, E.; Annis-Freeman, B.; Marvell, T. H.; LaVallie, E. R.; Zollner, R. S.; Bard, J.; Somers, W. S.; Stahl, M. L.; Kriz, R. W. A novel approach to identifying β -secretase inhibitors: Bis-statine peptide mimetics discovered using structure and spot synthesis. *Peptides (N. Y., NY, U. S.)* **2006**, *27*, 1877–1885.

(30) Vonrhein, C.; Flensburg, C.; Keller, P.; Sharff, A.; Smart, O.; Paciorek, W.; Womack, T.; Bricogne, G. Data processing and analysis with the *autoPROC* toolbox. *Acta Crystallogr., Sect. D: Biol. Crystallogr.* **2011**, *67*, 293–302.

(31) Kabsch, W. XDS. *Acta Crystallogr., Sect. D: Biol. Crystallogr.* **2010**, *66*, 125–132.

(32) (a) French, S.; Wilson, K. On the treatment of negative intensity observations. *Acta Crystallogr., Sect. A: Cryst. Phys., Diffr., Theor. Gen. Crystallogr.* **1978**, *A34*, 517–525. (b) Collaborative computational project, number 4. The CCP4 suite: programs for protein crystallography. *Acta Crystallogr., Sect. D: Biol. Crystallogr.* **1994**, *50*, 760–763.

(33) Murshudov, G. N.; Vagin, A. A.; Dodson, E. J. Refinement of macromolecular structures by the maximum-likelihood method. *Acta Crystallogr., Sect. D: Biol. Crystallogr.* **1997**, *D53*, 240–255.

(34) Bricogne, G.; Blanc, E.; Brandl, M.; Flensburg, C.; Keller, P.; Paciorek, W.; Roversi, P.; Smart, O. S.; Vonrhein, C.; Womack, T. O. *BUSTER*; Global Phasing Ltd: Cambridge, UK, 2011.

(35) Emsley, P.; Cowtan, K. *Coot*: model-building tools for molecular graphics. *Acta Crystallogr., Sect. D: Biol. Crystallogr.* **2004**, *D60*, 2126–2132.

(36) Adams, P. D.; Afonine, P. V.; Bunkoczi, G.; Chen, V. B.; Davis, I. W.; Echols, N.; Headd, J. J.; Hung, L.-W.; Kapral, G. J.; Grosse-Kunstleve, R. W.; McCoy, A. J.; Moriarty, N. W.; Oeffner, R.; Read, R. J.; Richardson, D. C.; Richardson, J. S.; Terwilliger, T. C.; Zwart, P. H. PHENIX: a comprehensive Python-based system for macromolecular structure solution. *Acta Crystallogr., Sect. D: Biol. Crystallogr.* **2010**, *66*, 213–221.